

**Title: Toxin resistance mechanisms span biological scales in the Royal Ground Snake  
*Erythrolamprus reginae***

**Authors:** V. Ramírez-Castañeda<sup>1\*</sup>, S. A. Nixon<sup>2</sup>, D Alarcón-Naforo<sup>3</sup>, F. Abderemane-Ali<sup>4</sup>, R. W. Fitch<sup>5</sup>, D. Salazar-Valenzuela<sup>6</sup>, D. L. Minor, Jr.<sup>2,7,8,9,10</sup>, R. D. Tarvin<sup>1\*</sup>

**Affiliations:**

<sup>1</sup>Museum of Vertebrate Zoology and Department of Integrative Biology, University of California, Berkeley, CA, 94720, USA

<sup>2</sup>Cardiovascular Research Institute, University of California, San Francisco, CA, 94158

<sup>3</sup>Departamento de Biología, Facultad de Ciencias, Universidad Nacional de Colombia, Bogotá, Colombia

<sup>4</sup>Department of Physiology, David Geffen School of Medicine, University of California, Los Angeles, CA, 90095, USA

<sup>5</sup>Department of Chemistry and Physics, Indiana State University, Terre Haute, IN, 47809, USA

<sup>6</sup>Centro de Investigación de la Biodiversidad y Cambio Climático (BioCamb) e Ingeniería en Biodiversidad y Recursos Genéticos, Facultad de Ciencias de Medio Ambiente, Universidad Tecnológica Indoamérica, Av. Machala y Sabanilla, Quito, Ecuador

<sup>7</sup>Departments of Biochemistry & Biophysics, and Cellular & Molecular Biology, University of California, San Francisco

<sup>8</sup>California Institute for Quantitative Biomedical Research, University of California, San Francisco

<sup>9</sup>Kavli Institute for Fundamental Neuroscience, University of California, San Francisco

<sup>10</sup>Molecular Biophysics and Integrated Bio-imaging Division, Lawrence Berkeley National Laboratory, Berkeley, CA

\*Corresponding author. Email: [vramirez@berkeley.edu](mailto:vramirez@berkeley.edu), [rdtarvin@berkeley.edu](mailto:rdtarvin@berkeley.edu)

**Abstract:** Exposure to multiple toxins imposes selection that should result in diverse resistance strategies. We studied the pan-Amazonian snake *Erythrolamprus reginae* (Colubridae), which preys on poisonous frogs, to evaluate toxic prey consumption and resistance. Feeding assays revealed that prey toxicity imposes costs that influence foraging strategies, yet liver proteins restored sodium channel activity inhibited by poison frog alkaloids, and transcriptomic profiling revealed liver-specific upregulation of transporters after poison frog ingestion. Additionally, the *E. reginae* voltage-gated sodium channel Na<sub>v</sub>1.4 is highly resistant to guanidium toxins but not to poison frog alkaloids. These findings demonstrate that *E. reginae* is adapting to a chemically diverse diet by evolving multiple overlapping and complementary forms of resistance, providing unparalleled insight into physiological and evolutionary implications of whole-organismal toxin resistance.

## Main Text:

### Introduction

Small-molecule toxins often exert strong effects in ecological interactions, mostly by serving as chemical defenses against predation or herbivory (1, 2). Exposure to multiple toxins imposes diverse selective pressures, potentially leading to a toxin-resistant phenotype that operates across biological levels (3). Predators of amphibians, for example, have to counteract multiple chemicals secreted from different species or even the same individual (4–6). As a result, some predators avoid toxic prey. However, others have evolved to resist toxins through multiple behavioral, physiological, and molecular adaptations (3). Understanding such traits requires an integrative approach because of the inherent system complexity.

The pan-Amazonian Royal Ground snake *Erythrolamprus reginae* (Squamata: Colubridae) is a generalist predator that consumes multiple species of poisonous frogs (Bufonidae and Dendrobatidae families) that have a diverse set of steroidal and alkaloid defenses (Albarelli and Santos-Costa 2010; Pašukonis and Loretto 2020). *E. reginae* harbors substitutions in voltage-gated sodium channels ( $\text{Na}_v$ ) that provide target-site resistance (TSR) to two guanidinium toxins: tetrodotoxin (TTX), which is present in some bufonids, and saxitoxin (STX), for which a local source is unknown (7). In addition, many snakes are not sensitive to the effects of the steroidal toxins (e.g., bufadienolides) because of TSR mutations in their sodium-potassium pumps (8, 9). Resistance mechanisms to other alkaloids present in poisonous frogs is largely uncharacterized. Thus, toxin resistance in *E. reginae* likely involves additional mechanisms such as the upregulation of xenobiotic enzymes, the formation of diffusion barriers, or toxin-binding proteins (reviewed by (3)). The last strategy has been documented in frogs for saxitoxin (STX) via the STX-binding protein saxiphilin (Sxph) and for STX and tetrodotoxin (TTX) in pufferfish via the pufferfish saxitoxin and tetrodotoxin binding protein (PSTBP) (10–14). Radiolabelled STX binding studies have also suggested the presence of STX-binding proteins in reptiles, amphibians, fish, and arthropods (3, 15). Yet, resistance mechanisms for the vast majority of naturally occurring toxins remain unknown, especially for predators such as snakes that are both elusive and scarce.

Here we aim to unravel the complexity of toxin resistance in *E. reginae* by investigating several biological scales where toxins may influence the evolution of resistant traits, from behavioral decisions to the suite of possible molecular resistance mechanisms. We employ multiple methods to investigate this paradigm by: 1) observing predation behavior to assess interactions with toxic prey; 2) investigating the expression of detoxifying proteins in several organs, and 3) evaluating the resistance conferred by TSR against different toxins present in the snake's diet. Our findings offer a compelling and comprehensive example of how predators adapt to diverse toxic pressures, revealing the physiological and evolutionary complexity of toxin resistance.

### Results and Discussion

### ***E. reginae* snakes exhibit avoidance and specific behaviors when feeding on the toxic poison frog *Ameerega trivittata***

While toxic prey are traditionally considered a low-quality food due to energetic trade-offs between prey nutrition and harmful effects of toxins (16–23), and many studies assume that predators avoid toxic prey, some predators such as *E. reginae* clearly do not, possibly because the trade-off between nutrition and toxicity may be minimized for resistant predators. Most toxic prey studies, outside herbivory research, focus on lab-trained predators or clay models (24–26), yet little is known about predator behavior in natural settings, especially in vertebrates. Bridging this gap can help connect theoretical and experimental approaches with real-world ecological interactions.

We tested for behavioral avoidance by offering adult *E. reginae* snakes from Leticia, Amazonas, Colombia (Data S6) (fasted for five days) a set of locally co-occurring frog prey with diverse chemical defenses and toxicity levels. The only highly toxic frog included was the dendrobatid *Ameerega trivittata*, which secretes histrionicotoxins (HTX), pumiliotoxins (PTX), and decahydroquinolines (DHQ) (4, 27), and is a known prey item of *E. reginae* (28). The other frogs included putatively non-toxic hylid species, primarily *Scinax ruber*, as well as *Dendropsophus* sp. and *Sphaenorhynchus lacteus*. Additionally, some snakes were offered mildly toxic frogs, *Leptodactylus* sp. and *Rhinella margaritifera*, which secrete amines and steroidal toxins (respectively) (29–31). Chemical analysis using gas chromatography mass spectrometry (GC-MS) confirmed the presence of multiple neurotoxic alkaloids from whole skins of *A. trivittata* ( $n = 6$ ), including DHQs, N-methyl-DHQs, 5,8-indolizidines, and HTXs, but not *S. ruber* ( $n = 6$ ); other species were not tested.

When offered *A. trivittata*, only 4 of 10 snakes were willing to eat, and one died after ingestion (Fig. 1A-B, Data S1-S2). If the snake did not consume *A. trivittata* within two hours, we then removed the *A. trivittata* and offered another prey option (*S. ruber*, *Dendropsophus* sp., *Sphaenorhynchus lacteus*, *Leptodactylus* sp., or *R. margaritifera*). All 6 of the snakes that refused to consume *A. trivittata* consumed the second prey that was offered, usually within one minute. Snakes also showed significant differences in the handling and consumption of *A. trivittata* versus other prey by taking longer to swallow them (Fig. 1C) and exhibiting a unique "dragging" behavior—rubbing the frog along the ground (see video Data S2 and YouTube (<https://youtube.com/shorts/CUsNjgG3jTA?feature=share>)). This behavior was exclusively observed during ingestion of *A. trivittata* (Fig. 1D). We hypothesize that rubbing the frog on the ground may help remove or break down some of the toxins. Similar behaviors such as dragging, wiping, or washing, have been reported in the hooded merganser (*Lophodytes cucullatus*), the southern ground hornbill (*Bucorvus leadbeateri*), and the grey heron (*Ardea cinerea*) when feeding on frogs and toxic newts (32–34). Thus, increased time and/or energy is expended when handling highly toxic prey (35).

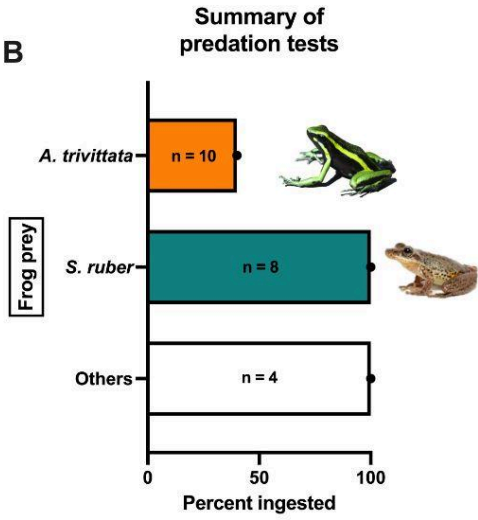
Our findings demonstrate behavioral avoidance of *A. trivittata* by *E. reginae* and underscore challenges posed by toxic prey at the organismal level, as reflected in distinct behavioral responses and survival outcomes. Optimal foraging theory predicts that predators may consume toxic prey when the alternative is less nutritious (21, 36) or more difficult to locate (37). However, multiple factors influence this type of foraging behavior, including physiological state: starved predators are more likely to consume toxic prey (38), and well-fed predators tend to make decisions based on prior experiences (39). Therefore, profitability is not a binary variable

but instead an integration of physiology, prey community, toxin resistance, and prior experience, and even when animals might possess some resistance to toxins, they may still endure significant energetic and opportunity costs.

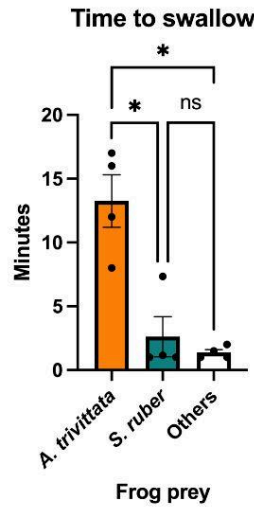
A



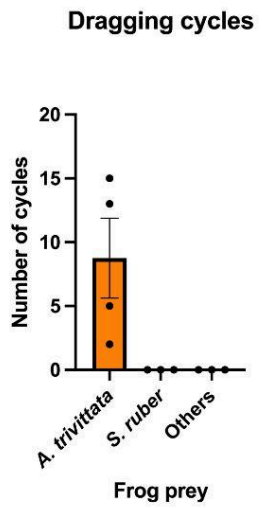
B



C



D



E

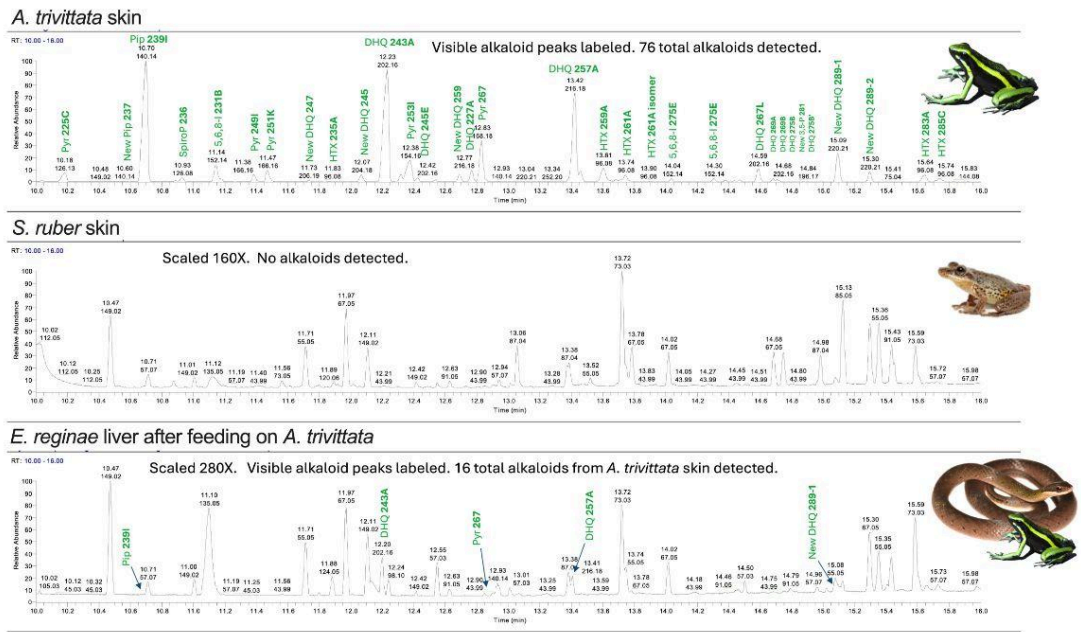


**Fig. 1. *E. reginae* presented longer swallowing times and a dragging behavior when feeding on the poisonous frog *Ameerega trivittata*.** (A) *Erythrolamprus reginae* feeding on a three-striped poison frog (*A. trivittata*), photographed by Leonardo Castañeda. (B) Summary of predation trials and ingestion percentages. *A. trivittata* (high alkaloid content) was offered to *E. reginae* 10 times, of which only four frogs were consumed. One snake died after *A. trivittata* ingestion. *S. ruber* (no alkaloids) was offered eight times, and all were consumed, as well as four individuals of other frog species (1 *Dendropsophus* sp., 1 *Leptodactylus* sp., 1 *Rhinella margaritifera* and 1 *Sphaenorynchus lacteus*) that were offered. (C) Comparison of swallowing time between *E. reginae* feeding on *A. trivittata*, *S. ruber*, and other species revealed a significant difference (Kruskal-Wallis test; \*,  $P \leq 0.05$ ). (D) Analysis of drag cycle behavior during predation revealed that this behavior was exhibited only when feeding on *A. trivittata*. In contrast, no such behavior was observed when feeding on *S. ruber* or other species. (E) GC-MS example result from an *A. trivittata* skin, *S. ruber* skin, and *E. reginae* liver after feeding on *A. trivittata*.

### **Soluble liver proteins contribute to *E. reginae* ability to consume *A. trivittata***

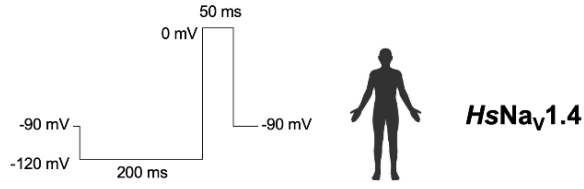
Once toxin ingestion occurs, predators rely on resistance mechanisms that involve metabolizing the toxin and/or modifying its target (3). We endeavored to identify proteins implicated in toxin resistance in the liver, the primary organ responsible for detoxification. Given the enormous diversity of toxic compounds present in frogs, we chose to focus on a subset that act on  $\text{Na}_v$  channels (27). We first established their activity on the human skeletal muscle  $\text{Na}_v$  channel (*HsNa<sub>v</sub>1.4*) using semi-automated planar patch-clamp electrophysiology in mammalian cells. Half-maximal inhibitory ( $\text{IC}_{50}$ ) values were in line with previous studies (Fig. S2) (40, 41). We also present the first  $\text{Na}_v$  electrophysiological data for several alkaloids unique to poison frogs: histrionicotoxin (HTX) **283A**, H<sub>8</sub>-HTX, decahydroquinoline (DHQ) **167**, and DHQ **195A**, *A. trivittata* skin secretion (diluted 1:200), and pumiliotoxin **251D** (PTX **251D**), which has been previously studied (42). We selected concentrations sufficient to block approximately 90% of the *HsNa<sub>v</sub>1.4* current (neoSTX: 1.5 nM, STX: 100 nM, TTX: 300 nM). Due to scarce material and the lower affinity against *HsNa<sub>v</sub>1.4*, poison frog toxins were tested at single concentrations sufficient to block *HsNa<sub>v</sub>1.4* by at least 60%: PTX **251D**, 500  $\mu\text{M}$ ; H<sub>8</sub>-HTX, 250  $\mu\text{M}$ ; HTX **283A**, 500  $\mu\text{M}$ .

We then developed a novel assay for screening liver tissue for toxin neutralization activity. We pre-treated toxins with *E. reginae* liver extract (0.2 mg/mL final concentration) for 30 minutes at room temperature, to allow any proteins to bind to or modify the toxins. We then used semi-automated planar patch-clamp electrophysiology to compare *HsNa<sub>v</sub>1.4* currents sequentially elicited under saline (baseline), toxin, incubated toxin:liver extract, and finally liver extract (Fig. S3). Restoration of channel activity in the presence of the incubated toxin:liver extract, relative to baseline and toxin-alone block, was interpreted as evidence for detoxifying or toxin-binding proteins in the liver (Fig. 2). *E. reginae* liver extracts were compared against liver extracts from two control (toxin-sensitive) species: the house mouse (*Mus musculus*) and another snake, *Contia tenuis*, a North American colubrid with no known natural exposure to dendrobatid alkaloids. None of the tested liver extracts significantly inhibited *HsNa<sub>v</sub>1.4* currents when applied alone (Fig. 2B, Fig. S4 and S5). Remarkably, preincubation of *E. reginae* liver extract ameliorated the effects of all poison frog alkaloids tested, with the greatest current recovery observed for HTX **283A** (mean  $76.3 \pm 9.1\%$ , Fig. 2B), representing the first known resistance

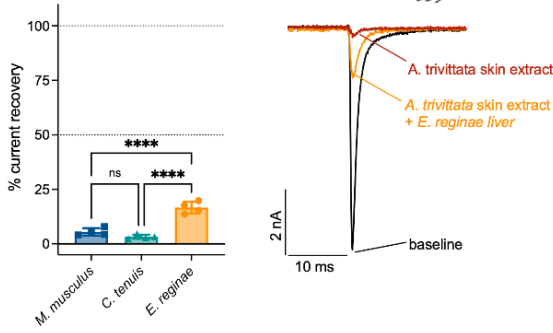
mechanism to HTX. This effect also extended to *A. trivittata* skin extract ( $16.6 \pm 2.7\%$ , Fig. 2A) and neoSTX ( $61.1 \pm 6.0\%$ , Fig. 2F), but not to TTX or STX. By contrast, mouse liver extract did not restore sodium channel activity for any toxin (Fig. 2 and Fig. S4), indicating that amelioration of the toxin block was not driven by general vertebrate liver detoxification enzymes. Similarly, *C. tenuis* liver extract had no effect on any dendrobatid toxin, STX, or TTX, but it completely ameliorated block by neoSTX ( $91.5 \pm 7.4\%$ ) (Fig. 2F and Fig. S5). These findings suggest that liver detoxification of neoSTX may be common in snakes, but that *E. reginae* liver detoxification activity is also ecologically specific, targeting toxins present in *A. trivittata*. Interestingly, the inability of *E. reginae* liver extracts to affect *HsNa<sub>v</sub>1.4* block by STX or TTX suggest that *E. reginae* relies on alternative resistance strategies for these compounds.

Although *E. reginae* liver extract reduced the inhibitory effects of PTX **251D**, H<sub>8</sub>-HTX, HTX **283A**, and *A. trivittata*, some block remained (Fig. 2). This suggests that while the liver may reduce the impact of these toxins, there may still be some physiological cost associated with consuming *A. trivittata*, which may explain the snakes' reduced preference for this diet. Alternatively, the high concentrations of dendrobatid toxins used in the present study (250–500  $\mu$ M) may have exceeded the neutralizing capacity of the liver. Additionally, while *E. reginae* liver had no effect on TTX and STX, it restored the majority of *HsNa<sub>v</sub>1.4* current from the closely related structural analogue neoSTX (Fig. 2F). Due to limited toxin and liver material, we were unable to test varying ratios of toxin:liver extract to explore potential limits of this mechanism. It would also be of interest to explore other higher affinity pharmacological targets of dendrobatid toxins, such as nicotinic acetylcholine receptors for HTX. Increasing the incubation time for the liver:toxin extracts may also further modulate the toxin effects. Additionally, gene expression related to detoxification may vary under different conditions, potentially increasing the liver's detoxifying capacity in response to toxin exposure. This is particularly relevant since the tissues used in this study were obtained from fasting snakes, rather than from individuals exposed to toxins.

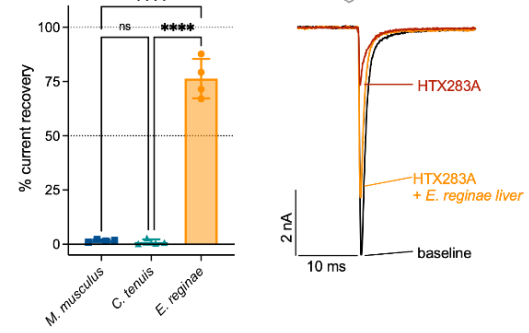
While total protein amount was standardized for these assays, the identity, relative abundance and affinities of the proteins contributing to detoxification are currently unknown. Further, we cannot exclude the possibility that the stability or functionality of potential toxin-binding proteins may have been impaired or lost during extraction. Since no detergents were used during either the protein extraction or toxin incubation in the liver neutralization assay, it likely primarily captured soluble candidate proteins while excluding membrane proteins. Further work is therefore needed to identify and characterize these proteins. Nonetheless, it is remarkable that *E. reginae* liver extracts uniquely modulated toxin activity, underscoring liver detoxification as a key mechanism of toxin resistance for *E. reginae*.



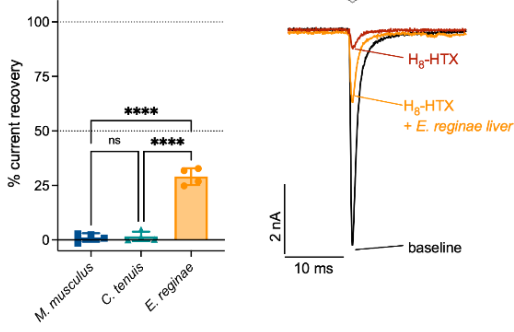
**A A. trivittata skin extract**



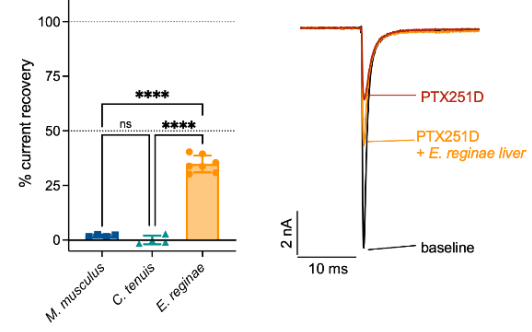
**B HTX283A**



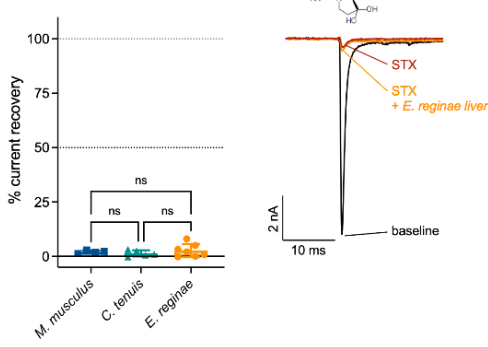
**C H<sub>8</sub>-HTX**



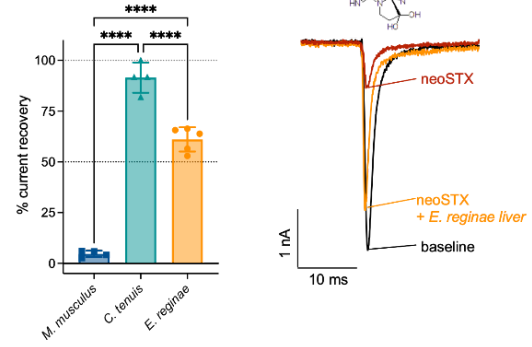
**D PTX251D**



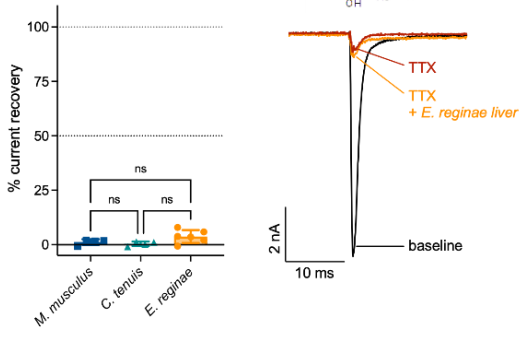
**E STX**



**F neoSTX**



**G TTX**



**H Liver alone**

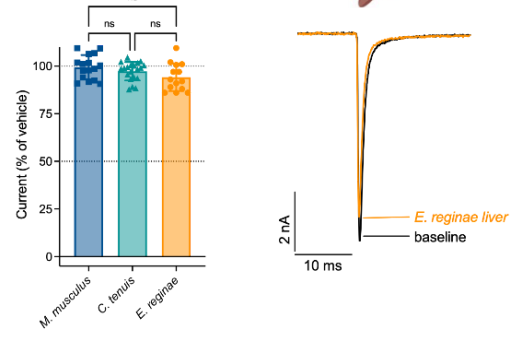




**Fig. 2. *E. reginae* liver extract mitigates dendrobatid toxin and neoSTX block of *HsNa<sub>v</sub>1.4*, providing evidence of liver proteins involved in detoxification.** Concentrations used: (A), *A. trivittata* skin extract, diluted 1:200; (B), HTX 283A, 500  $\mu$ M; (C), H<sub>8</sub>-HTX, 250  $\mu$ M; (D), PTX 251D, 500  $\mu$ M; (E), STX, 100 nM; (F), neoSTX, 1.5 nM; (G), TTX, 300 nM; (H), liver extract alone, 0.2 mg/mL. For all toxins and extracts, exemplar whole-cell patch-clamp recordings of *HsNa<sub>v</sub>1.4* expressed in CHO cells are plotted in the absence of toxin (baseline, black), presence of toxin alone (maroon), and toxin mixed with *E. reginae* liver extract (orange). Current recovery with liver-treated toxin relative to baseline and toxin alone, for *E. reginae* liver (orange), *C. tenuis* liver (teal), and mouse liver (blue). Each point represents a single cell ( $n$  = minimum of 4 cells) and error bars represent standard deviation. Asterisks represent statistically significant differences in toxin current recovery between extracts ( $p$  < 0.0001, one-way ANOVA with Tukey's post hoc test).

### High expression of transporter-related proteins in the liver is associated with *A. trivittata* consumption

Following prey ingestion, resistance can also be modulated by increased expression of specific genes involved in toxin breakdown, binding, and clearance (3). To identify specific molecular candidates that mediate detoxification, we generated transcriptomes from four digestive tissues (tongue, stomach, liver, and gut) in *E. reginae* that had consumed *A. trivittata* ( $n$  = 3), *Scinax ruber* ( $n$  = 3), or were fasting ( $n$  = 3) (Data S7). Expression profiles clustered primarily by tissue, with tongue being most distinct (Fig. S6A–B). The greatest number of upregulated genes was observed in response to *A. trivittata* consumption, with the liver showing the strongest transcriptional response among the tissues (Fig. 3A–B). In contrast, *S. ruber* elicited the weakest transcriptional activation. Fasting snakes show upregulation of some genes, particularly in the stomach, likely related to canonical responses to starvation (43).

As liver extracts from fasting *E. reginae* neutralized *A. trivittata* toxins, we reviewed genes upregulated in the liver after consuming *A. trivittata* to identify candidate genes underlying neutralization. Literature suggests several soluble proteins may contribute to toxin neutralization, including serpins (44), transferrin-like proteins (*TF*, *TFRC*, *TFR2*, *TFIP11*) (45, 46), and lactotransferrin-like proteins (LOC139173594) (47). However, none of these genes were upregulated in the *A. trivittata* treatment. One, however, showed significant upregulation (*SERPIN6*, adjusted  $p$ -value < 0.05) in snakes fed *S. ruber* (Fig. S6C). Gene Ontology (GO) analyses did not detect enrichment of soluble proteins (Fig. S6D). Nonetheless, many soluble proteins that could contribute to toxin neutralization were expressed in all liver transcriptomes, suggesting that presence, rather than overexpression, of toxin-binding proteins may be sufficient for functional resistance. Alternatively, some toxin-binding proteins may remain uncharacterized, potentially corresponding to unannotated LOC genes that were upregulated (see Data S3) (44).

Focusing on liver-specific responses to consumption of *A. trivittata*, GO analyses revealed significant enrichment of membrane-bound proteins involved in transport activity (Fig. 3C). Among the most upregulated genes were members of the solute carrier (SLC) family, widely known for absorption, uptake, and clearance of xenobiotics and drugs (48, 49) (Fig. S6C). For

example, the upregulated gene *SLC22A7* encodes a known organic anion transporter involved in hepatic excretion of toxins and metabolites in humans, including the plant and amphibian pyrrolizine toxins (49–51). Other upregulated solute carriers included *SLC15A1*, involved in peptidomimetic uptake (52), and transporters such as *SLC1A5*, *SLC16A6*, and *SLC5A12*, linked to amino acid and monocarboxylate metabolism (49). While many of these transporters exhibit substrate overlap and species-specific variability, their roles in xenobiotic handling make them strong candidates for toxin clearance (48). This multifunctionality of SLC transporters warrants further investigation, especially considering that non-synonymous mutations in SLC genes have been linked to altered substrate specificity and efficiency (53–55). Such mutations may underlie evolutionary adaptations that enable predators like *E. reginae* to regularly consume chemically defended prey without succumbing to their most toxic effects.

Other genes involved in transport were also overexpressed in *E. reginae* after consumption of *A. trivittata*. These include *ABCA12* and *NPC1L1*, known lipid and cholesterol transporters (56, 57). Given their role in lipophilic molecule transport, these proteins may contribute to the movement of hydrophobic toxins such as HTX and PTX. The upregulated RAB11FIP1, a protein involved in the regulation of intracellular transport vesicles, may play a role in facilitating toxin engulfment, intracellular trafficking, and eventual elimination, potentially contributing to the cellular handling of toxic compounds (58).

Beyond direct detoxification, transporters also play essential roles in maintaining systemic homeostasis. Their increased expression in response to *A. trivittata* ingestion may reflect a broader metabolic stress response, involving inter-organ signaling and physiological adaptation (48). Supporting this idea, we observed overexpression of heat shock proteins in the *A. trivittata* treatment, including *HSPA2* and its associated regulator *HSPBAP1* (59) (Fig. S6C). The phospholipase *PLA2G7*, a gene found in the venom of various organisms such as snakes, bees, and scorpions, as well as the sphingosine-1-phosphate plasma transporter *MFSD2B*, were also highly expressed and are known to be involved in inflammatory responses (60–64) (Fig. S6C). These proteins are well-established markers of cellular stress and may signal a generalized physiological response to toxic prey ingestion.

Altogether, our RNA-seq data suggest that transporter overexpression in the liver represents a complementary resistance mechanism of toxin elimination. While no previously reported toxin-binding proteins were strongly upregulated after *A. trivittata* consumption, the presence of soluble candidates and upregulation of transmembrane transporters indicate that multiple pathways, including toxin binding, membrane trafficking, and metabolic elimination, jointly contribute to toxin resistance in *E. reginae*.

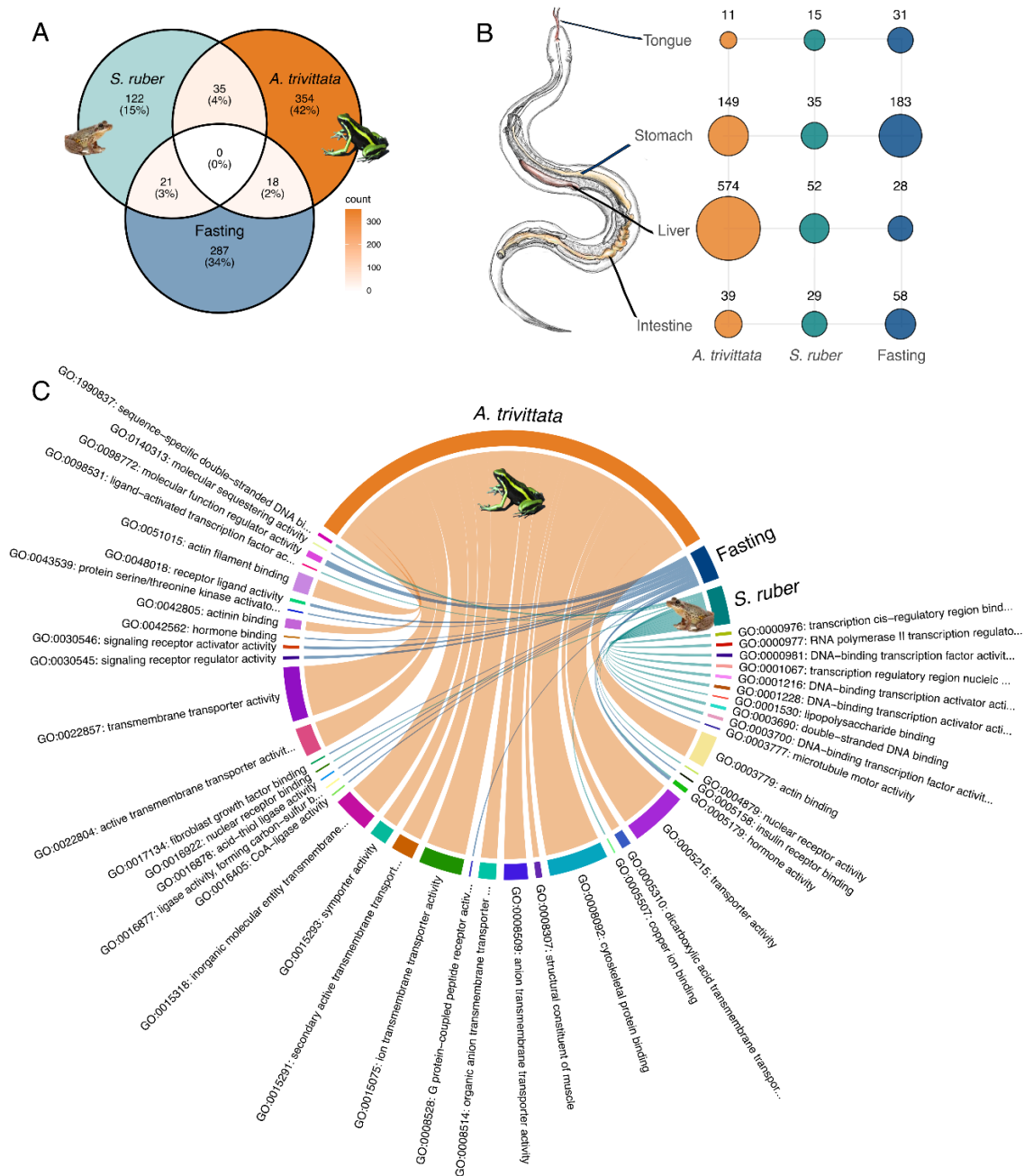


**Fig. 3. Consumption of *A. trivittata* changes liver gene expression in *E. reginae* more than in other conditions and induces high expression of transporter genes.** (A) Venn diagram showing the overlap of upregulated protein-coding transcripts across three conditions after differential expression analysis between fasting vs. *A. trivittata*, fasting vs. *S. ruber*, and *S. ruber* vs. *A. trivittata* of the combined digestive system tissues (tongue, stomach, liver, and intestine). (B) Number of upregulated protein-coding transcripts in each digestive tissue after differential expression analysis between fasting vs. *A. trivittata*, fasting vs. *S. ruber*, and *S. ruber* vs. *A. trivittata*. Snake diagram was drawn by Bernardo Moreno Peniche. (C) Circular plot representing the upregulated liver Gene Ontology (GO) enrichment analysis (molecular function category)

using topGO in *E. reginae* across the three conditions. Each segment represents a GO term. The width of each segment corresponds to the "Significant" value, indicating the number of upregulated genes associated with each GO term.

### **Some *E. reginae* voltage-gated sodium channel alleles (Na<sub>v</sub>1.4) are highly resistant to tetrodotoxin, saxitoxin, and neo-saxitoxin**

The final frontier of toxin resistance is at the toxin target itself. If the toxin reaches its target, amino acid substitutions can decrease or prevent toxin binding—a mechanism known as target-site resistance (TSR) (8, 65–71). Putative TSR has been previously identified in Na<sub>v</sub> sequences of *Erythrolamprus* snakes (7, 72). In some *E. reginae* populations, Na<sub>v</sub> channels exhibit amino acid substitutions at sites experimentally reported to confer tetrodotoxin (TTX) resistance in Na<sub>v</sub>1.1, Na<sub>v</sub>1.3, Na<sub>v</sub>1.4, Na<sub>v</sub>1.6, and Na<sub>v</sub>1.8 (7, 65, 73, 74).

The evolution of TSR in the muscle-expressed Na<sub>v</sub>1.4 sodium channel is closely associated with toxin resistance in organisms exposed to high levels of TTX and STX (7). However, physiological experiments are necessary to confirm whether amino acid substitutions actually alter toxin sensitivity or affect protein function (69). We tested the hypothesis that TSR-associated substitutions in *E. reginae* Na<sub>v</sub>1.4 reduce channel sensitivity to guanidinium neurotoxins. To do so, we examined two variants: a putative resistant variant (*ErNa<sub>v</sub>1.4-R*), which harbors TTX TSR-associated substitutions, and a non-resistant variant (*ErNa<sub>v</sub>1.4-NR*) lacking these mutations, as described in (7) (Fig. S1, Data S4). The resulting experiments provide the most comprehensive electrophysiological data for a snake Na<sub>v</sub> channel to date.

*ErNa<sub>v</sub>1.4-R* includes five amino acid substitutions at functionally relevant sites (Fig. S1); at least two of them, D1539N and G1540D, have been characterized as conferring TTX resistance in other species (65, 74, 75). Using two-electrode voltage-clamp (TEVC) recordings in *Xenopus laevis* oocytes, we compared the toxin responses of *ErNa<sub>v</sub>1.4-R* and *ErNa<sub>v</sub>1.4-NR*, alongside the human Na<sub>v</sub>1.4 (*HsNa<sub>v</sub>1.4*) channel as a control. These recordings, performed under single-stimulus protocols, allowed us to assess the extent to which the substitutions in the *ErNa<sub>v</sub>1.4-R* variant contribute to toxin resistance in *E. reginae*. Importantly, we synthesized the wild-type *E. reginae* Na<sub>v</sub>1.4 channels rather than introducing point mutations into a model organism sequence, preserving natural channel variation and its full response to toxin exposure. To provide a comprehensive characterization of *ErNa<sub>v</sub>1.4-R* and *ErNa<sub>v</sub>1.4-NR*, we evaluated basic electrophysiological properties such as activation and inactivation curves (Fig. S8), the half-maximal activation and inactivation voltages ( $V_{\text{activation}_{1/2}}$ —*ErNa<sub>v</sub>1.4-R*:  $-23.52 \text{ mV} \pm 3.554 \text{ mV}$ ; *ErNa<sub>v</sub>1.4-NR*:  $-22.98 \text{ mV} \pm 3.382 \text{ mV}$ ;  $V_{\text{inactivation}_{1/2}}$ —*ErNa<sub>v</sub>1.4-R*:  $-52.47 \pm 2.929$ ; *ErNa<sub>v</sub>1.4-NR*:  $-53.32 \pm 3.229$ ) (Fig. S8 and Table S3). Inactivation curves showed no differences, suggesting that the substitutions distinguishing the two variants do not affect inactivation, consistent with previous findings (76).

We conducted concentration–response curves for each toxin and found that the IC<sub>50</sub> values for *ErNa<sub>v</sub>1.4-R* are extremely high, in some cases, even the highest toxin concentrations applied had negligible effect on channel activity, making a precise IC<sub>50</sub> calculation impossible (Fig. 4, *ErNa<sub>v</sub>1.4-R* TTX & STX IC<sub>50</sub> >> 3000 nM; neoSTX IC<sub>50</sub> >> 333 nM; Fig. 3). In contrast, *ErNa<sub>v</sub>1.4-NR* exhibited a sensitivity profile closely aligned with that of *HsNa<sub>v</sub>1.4*, with the

following rank order: neoSTX > STX > TTX (Fig. 3,  $IC_{50}$  0.4048 nM  $\pm$  0.235 nM, 6.565 nM  $\pm$  1.013 nM, and 18.09  $\pm$  2.02 nM, respectively).  $IC_{50}$  values for *HsNa<sub>v</sub>1.4* are reported in Table S3. These results demonstrate that TSR in *ErNa<sub>v</sub>1.4-R* confers high resistance to TTX, STX, and neoSTX in *E. reginae*.

While five amino acid substitutions are present in *ErNa<sub>v</sub>1.4-R*, not all are likely to contribute equally to the observed resistance. The substitutions D1539N and G1540D, located in the domain IV p-loop (selectivity filter), are well-characterized TSR substitutions previously shown to confer high TTX resistance (65, 74, 75), and likely represent the primary contributors to the STX and TTX-resistant phenotype in *E. reginae* as shown in the structural models (Fig. 4M–P). An additional substitution, P1550S, also occurs in this region and is found in dendrobatid frogs, though its functional role remains unclear. Structural modeling (Fig. 4M–P) shows that the remaining substitutions, I425L (domain I, segment 6) and S725N (domain II, segment 5), are located on the outer face of the pore domain, making it unlikely that they directly affect STX or TTX binding. Notably, S725N is also found in highly TTX-resistant species such as *Heterodon platirhinos* and *Thamnophis sirtalis* (Willow Creek population), despite not being previously identified as a TSR site (7, 77). Together, these data suggest that while five substitutions are present, resistance is most parsimoniously explained by the convergent D1539N and G1540D mutations in the domain IV p-loop, consistent with findings from other resistant lineages (65, 74).

These guanidinium toxins are common across various ecosystems but have not yet been documented in the known diet or habitat of *E. reginae* (7, 78). The extreme resistance observed in some individuals suggests that populations of *E. reginae* may be exposed to high concentrations of one or more of these toxins (7, 79). Because GC–MS cannot detect TTX, its presence in *A. trivittata* cannot be ruled out. Interestingly, neoSTX appears to be counteracted by two independent resistance mechanisms: liver-expressed proteins that neutralize the toxin (Fig. 2F) and TSR-associated mutations in *Na<sub>v</sub>1.4*. Although we initially hypothesized that this redundancy evolved in response to the extreme potency of neoSTX ( $IC_{50}$  < 1 nM), STX is also a low-nanomolar blocker, making a strictly potency-based explanation less conclusive. Moreover, the added protection conferred by liver-mediated detoxification, despite the strong TSR-mediated resistance, raises the possibility that neoSTX may have an additional, unidentified molecular target.

Our findings confirm the coexistence of multiple resistance mechanisms in *E. reginae* from Leticia, Colombia. This population carries the *ErNa<sub>v</sub>1.4-R* variant and was also the source of liver samples used in recovery assays demonstrating the capacity to neutralize dendrobatid toxins and neoSTX (Data S5). Together, these results indicate that this population exhibits both TSR in *Na<sub>v</sub>1.4* and liver-mediated detoxification, highlighting the integrative nature of toxin resistance in this species and its ability to counteract complex chemical defenses.

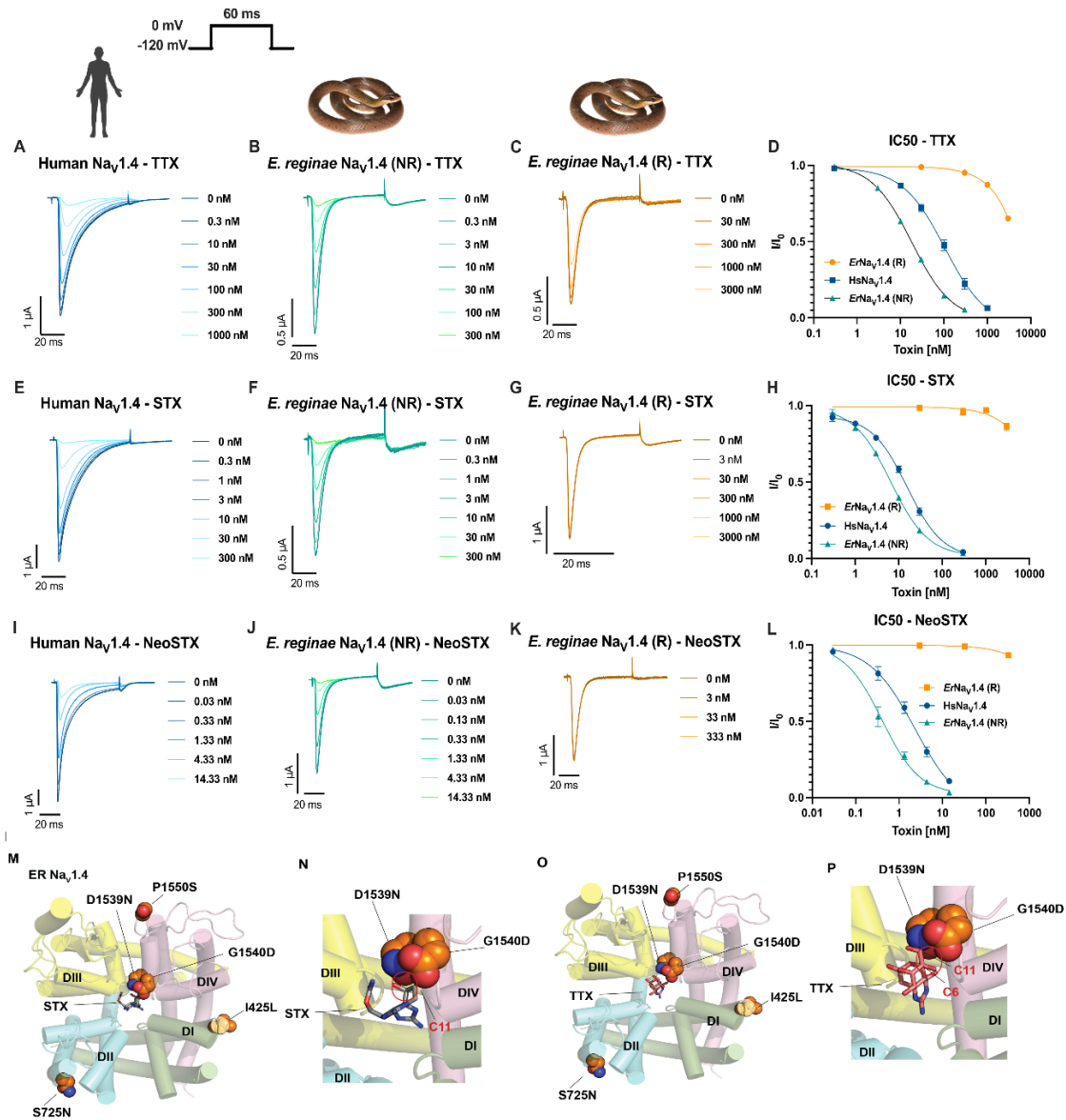


**Figure 4. Amino acid substitutions in *ErNa<sub>v</sub>1.4-R* confer high resistance to the neurotoxins TTX, STX, and neoSTX.** Exemplar recordings for Human Na<sub>v</sub>1.4 (*HsNa<sub>v</sub>1.4*, blue), *E. reginae* Na<sub>v</sub>1.4 non-resistant variant (*ErNa<sub>v</sub>1.4-NR*, green), and *E. reginae* Na<sub>v</sub>1.4 resistant variant (*ErNa<sub>v</sub>1.4-R* in orange) expressed in oocytes were exposed to increasing concentrations of TTX (A, B, C), STX (E, F, G) and neoSTX (I, J, K). Concentration-response curves were subsequently plotted for each Na<sub>v</sub> channel for TTX, STX, and neoSTX (D, H, L; respectively; for values, see Table S2). Each point represents mean normalized current with standard deviation ( $n = 6$ ). Note the different toxin concentrations used for *ErNa<sub>v</sub>1.4-R* (C, G, and K) compared to other graphs. Structural interactions of STX (M, N) and TTX (O, P) with a model of the *ErNa<sub>v</sub>1.4-R* variant. Residues shown in space-filling representation highlight the five amino acid substitutions at functionally relevant sites that differentiate *ErNa<sub>v</sub>1.4-R* and *ErNa<sub>v</sub>1.4-NR*.

Among these, only D1539N and G1540D appear to interact directly with the guanidinium toxins. Residue numbers correspond to the position in *HsNa<sub>v</sub>1.4*.

### ***E. reginae* Na<sub>v</sub>1.4-R is sensitive to *A. trivittata* toxins**

Na<sub>v</sub>1.4 has been identified as a key target of several toxins secreted by *A. trivittata*, including HTX and PTX (4, 27). To test for TSR to these toxins, we repeated the above experiments with isolated compounds found in *Ameerega* species, including histrionicotoxins (HTX **293A** and H<sub>8</sub>-HTX), pumiliotoxins (PTX **251D**), and decahydroquinolines (DHQ **167** and DHQ **195A**). We also compared responses to *A. trivittata* (toxic) and *S. ruber* skin secretions non-toxic (control). We also tested . Due to the scarcity of toxin material, we only used the *HsNa<sub>v</sub>1.4* as the control channel, and only assessed a single high concentration that allowed for sufficient repetitions to ensure statistical robustness in both *ErNa<sub>v</sub>1.4-R* and *HsNa<sub>v</sub>1.4*.

Unexpectedly, *ErNa<sub>v</sub>1.4-R* did not exhibit resistance to *A. trivittata* skin secretions, which significantly reduced the current by ~20% (Fig. 4C). The *S. ruber* secretion reduced currents by 5% (Fig. 5F). Although not statistically significant, the human channel showed a ~10% reduction in current following exposure to *A. trivittata* secretions (Fig 3C). To further validate these findings, we tested individual toxins found in *A. trivittata* and other dendrobatid frogs, including the alkaloids noted above (Fig. S7). Consistent with the whole-secretion current reductions, neither the *ErNa<sub>v</sub>1.4-R* nor *HsNa<sub>v</sub>1.4* exhibited resistance to any of these toxins, which caused ~10%-60% significant current reductions (Kruskal-Wallis test,  $P \leq 0.05$ ). These findings suggest that *E. reginae* relies on alternative toxin resistance mechanisms to consume *A. trivittata*, as discussed in previous sections. However, we cannot rule out the possibility that TSR in other targets plays a role, given that some *A. trivittata*-derived toxins are known to target channels beyond Na<sub>v</sub>1.4, such as nicotinic acetylcholine receptors (4, 27). Additionally, the concentrations used in this study for some of these toxins (Table S1) are exceedingly high compared to those typically encountered in nature, further suggesting that Na<sub>v</sub>1.4 may not be their primary target (80–82). Overall, our results indicate that TSR in *ErNa<sub>v</sub>1.4* is not the primary resistance mechanism against *A. trivittata* secretions but it is essential for resistance to TTX, STX, and neoSTX.

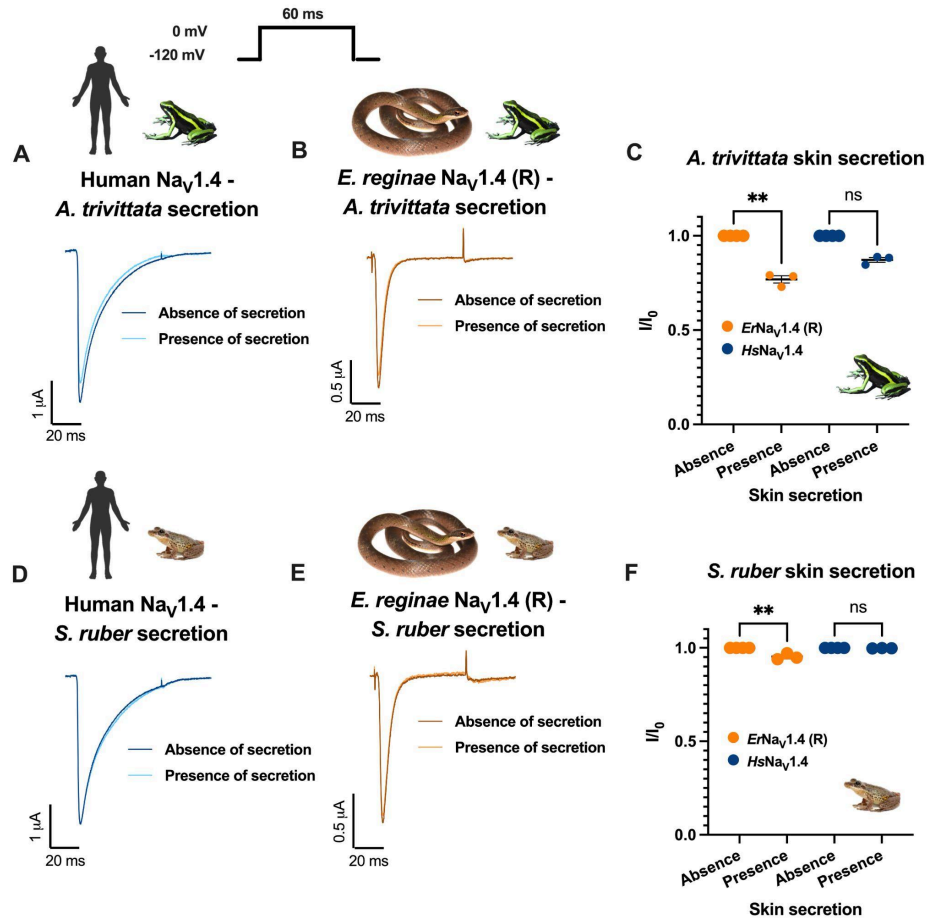


**Figure 5.** *ErNa<sub>V</sub>1.4-R* is sensitive to the *A. trivittata* poison frog skin secretions. Exemplar current recordings for *HsNa<sub>V</sub>1.4* (blue) and *ErNa<sub>V</sub>1.4-R* (orange) expressed in *X. laevis* oocytes and exposed to 1:1000 dilution of reconstituted skin secretions from *A. trivittata* (A, B) or *S. ruber* (D, E). Comparison of sodium current reduction in the presence or absence of *A. trivittata* (C) and *S. ruber* (F) skin secretions. Statistical significance was assessed using a Kruskal-Wallis test, with p-values provided for the corresponding comparisons. P-values are shown in the graph as (ns)  $P > 0.05$ ; (\*)  $P \leq 0.05$ ; (\*\*)  $P \leq 0.01$ ; (\*\*\*)  $P \leq 0.001$ .

## Conclusion

Here we present a multiscale investigation of toxin resistance in an elusive amazonian predator of poisonous frogs, the Royal Ground Snake *Erythrolamprus reginae*. We demonstrate that toxin resistance in *E. reginae* is not the result of a single trait but instead emerges from a dynamic integration of behavioral, physiological, and molecular adaptations. *E. reginae* exhibits behavioral avoidance towards toxic prey, despite demonstrating unique signatures of resistance to prey toxins. Mechanisms of resistance differed by toxin class, with TSR in voltage-gated sodium channels contributing to guanidinium alkaloid but not poison frog lipophilic alkaloid



resistance. In contrast, liver extracts were able to neutralize poison frog alkaloids but not guanidinium alkaloids, except for neoSTX. The presence of both mechanisms for neoSTX suggests strong selection for resistance to this toxin. Mysteriously, sources of STX, TTX, and neoSTX exposure are unknown for *E. reginae*, raising questions about the necessity of resistance, or alternatively our ignorance of the distributions of these toxins in the Amazon basin. Possible local sources of TTX include the Harlequin frogs (genus *Atelopus*) and flatworms; STX may occur in freshwater cyanobacteria that have yet to be identified in the Amazon. In summary, an integrative lens on the resistance phenotype has offered new insights into the depth of the physiological and behavioral consequences of consuming lethal neurotoxins. Adaptations to neurotoxins in animals such as *E. reginae* can inform drug design and help inspire novel treatments for cases of poisoning in humans.

## References and Notes

1. R. P. Ferrer, R. K. Zimmer, Molecules of Keystone Significance: Crucial Agents in Ecology and Resource Management. *BioScience* **63**, 428–438 (2013).
2. R. P. Ferrer, R. K. Zimmer, Community Ecology and the Evolution of Molecules of Keystone Significance. *The Biological Bulletin* **223**, 167–177 (2012).
3. R. D. Tarvin, K. C. Pearson, T. E. Douglas, V. Ramírez-Castañeda, M. J. Navarrete, The Diverse Mechanisms that Animals Use to Resist Toxins. *Annual Review of Ecology, Evolution, and Systematics* **54**, 283-306 (2023).
4. J. W. Daly, The chemistry of poisons in amphibian skin. *Proceedings of the National Academy of Sciences* **92**, 9–13 (1995).
5. J. W. Daly, Thirty Years of Discovering Arthropod Alkaloids in Amphibian Skin †. **3864**, 162–172 (1998).
6. R. A. Saporito, M. A. Donnelly, T. F. Spande, H. M. Garraffo, A review of chemical ecology in poison frogs. *Chemoecology* **22**, 159–168 (2011).
7. V. Ramírez-Castañeda, R. Tarvin, R. Marquez, Snakes (*Erythrolamprus* spp.) with a complex toxic diet show convergent yet highly heterogeneous voltage-gated sodium channel evolution. [Preprint] (2024). <https://doi.org/10.32942/X2MS6D>. [EcoEvoRxiv]
8. B. Ujvari, N. R. Casewell, K. Sunagar, K. Arbuckle, W. Wüster, N. Lo, D. O’Meally, C. Beckmann, G. F. King, E. Deplazes, T. Madsen, Widespread convergence in toxin resistance by predictable molecular evolution. *Proceedings of the National Academy of Sciences* **112**, 11911–11916 (2015).
9. S. Mohammadi, Z. Gompert, J. Gonzalez, H. Takeuchi, A. Mori, A. H. Savitzky, Toxin-resistant isoforms of Na<sup>+</sup>/K<sup>+</sup>-ATPase in snakes do not closely track dietary specialization on toads. *Proceedings of the Royal Society B: Biological Sciences* **283**, 20162111 (2016).

10. J. Mahar, G. L. Lukács, Y. Li, S. Hall, E. Moczydlowski, Pharmacological and biochemical properties of saxiphilin, a soluble saxitoxin-binding protein from the bullfrog (*Rana catesbeiana*). *Toxicon* **29**, 53–71 (1991).
11. M. A. Morabito, E. Moczydlowski, Molecular cloning of bullfrog saxiphilin: a unique relative of the transferrin family that binds saxitoxin. *Proceedings of the National Academy of Sciences* **92**, 6651 (1995).
12. M. Yotsu-Yamashita, A. Sugimoto, T. Terakawa, Y. Shoji, T. Miyazawa, T. Yasumoto, Purification, characterization, and cDNA cloning of a novel soluble saxitoxin and tetrodotoxin binding protein from plasma of the puffer fish, *Fugu pardalis*. *European Journal of Biochemistry* **268**, 5937–5946 (2001).
13. T.-J. Yen, M. Lolicato, R. Thomas-Tran, J. Du Bois, D. L. Minor, Structure of the saxiphilin:saxitoxin (STX) complex reveals a convergent molecular recognition strategy for paralytic toxins. *Science Advances* **5**, eaax2650 (2019).
14. Z. Chen, S. Zakrzewska, H. S. Hajare, A. Alvarez-Buylla, F. Abderemane-Ali, M. Bogan, D. Ramirez, L. A. O’Connell, J. Du Bois, D. L. Minor, Definition of a saxitoxin (STX) binding code enables discovery and characterization of the anuran saxiphilin family. *Proceedings of the National Academy of Sciences* **119**, e2210114119 (2022).
15. L. E. Llewellyn, P. M. Bell, E. G. Moczydlowski, Phylogenetic survey of soluble saxitoxin-binding activity in pursuit of the function and molecular evolution of saxiphilin, a relative of transferrin. *Proceedings of the Royal Society B: Biological Sciences* **264**, 891–902 (1997).
16. G. A. K. Marshall, On Diaposematism, with reference to some limitations of the Müllerian Hypothesis of Mimicry. *Transactions of the Royal Entomological Society of London* **56**, 93–142 (1908).
17. M. P. Speed, Muellierian mimicry and the psychology of predation. *Animal Behaviour* **45**, 571–580 (1993).
18. T. N. Sherratt, State-dependent risk-taking by predators in systems with defended prey. *Oikos* **103**, 93–100 (2003).
19. T. N. Sherratt, M. P. Speed, G. D. Ruxton, Natural selection on unpalatable species imposed by state-dependent foraging behaviour. *Journal of Theoretical Biology* **228**, 217–226 (2004).
20. J. Skelhorn, H. M. Rowland, J. Delf, M. P. Speed, G. D. Ruxton, Density-dependent predation influences the evolution and behavior of masquerading prey. *Proceedings of the National Academy of Sciences* **108**, 6532–6536 (2011).
21. C. G. Halpin, J. Skelhorn, C. Rowe, Predators’ decisions to eat defended prey depend on the size of undefended prey. *Animal Behaviour* **85**, 1315–1321 (2013).

22. J. Mappes, H. Kokko, K. Ojala, L. Lindström, Seasonal changes in predator community switch the direction of selection for prey defences. *Nature Communications* **5**, 5016 (2014).
23. H. M. Rowland, A. J. T. Fulford, G. D. Ruxton, Predator learning differences affect the survival of chemically defended prey. *Animal Behaviour* **124**, 65–74 (2017).
24. C. R. Darst, M. E. Cummings, Predator learning favours mimicry of a less-toxic model in poison frogs. *Nature* **440**, 208–211 (2006).
25. L. María Arenas, D. Walter, M. Stevens, Signal honesty and predation risk among a closely related group of aposematic species. *Science Reports* **5**, 11021 (2015).
26. C. G. Halpin, O. Penacchio, P. G. Lovell, I. C. Cuthill, J. M. Harris, J. Skelhorn, C. Rowe, Pattern contrast influences wariness in naïve predators towards aposematic patterns. *Science Reports* **10**, 9246 (2020).
27. J. C. Santos, R. D. Tarvin, L. A. O’Connell, “A Review of Chemical Defense in Poison Frogs (Dendrobatidae): Ecology, Pharmacokinetics, and Autoresistance” in *Chemical Signals in Vertebrates 13*, B. A. Schulte, T. E. Goodwin, M. H. Ferkin, Eds. (Springer International Publishing, Cham, 2016), pp. 305–337.
28. A. Pašukonis, M.-C. Loretto, “Predation on the Three-striped poison frog, *Ameerega trivitatta* (Boulenger 1884; Anura: Dendrobatidae), by *Erythrolamprus reginae* (Linnaeus 1758; Squamata: Collubridae)” (2020); <https://www.biotaxa.org/hn/article/view/60062>.
29. J. M. Cei, V. Erspamer, M. Roseghini, Taxonomic and Evolutionary Significance of Biogenic Amines and Polypeptides Occurring in Amphibian Skin. I. Neotropical Leptodactylid Frogs. *Systematic Biology* **16**, 328–342 (1967).
30. J. W. Daly, C. W. Myers, N. Whittaker, Further classification of skin alkaloids from neotropical poison frogs (Dendrobatidae), with a general survey of toxic/noxious substances in the amphibia. *Toxicon* **25**, 1023–1095 (1987).
31. I. Prates, M. M. Antoniazzi, J. M. Sciani, D. C. Pimenta, L. F. Toledo, C. F. B. Haddad, C. Jared, Skin glands, poison and mimicry in dendrobatid and leptodactylid amphibians. *Journal of Morphology* **273**, 279–290 (2012).
32. M. I. Kemp, A. C. Kemp, “Bucorvus and Sagittarius: Two Modes of Terrestrial Predation” in *Proceedings of the Symposium on African Predatory Birds* (Northern Transvaal Ornithological Society, Pretoria, 1978).
33. R. Underhill, “Mayne Island, B.C. Wetlands and Amphibian Habitats” (Mayne Island Conservancy Society, 2015).
34. C. Smith, J. Cranfield, S. J. Allain, ‘Stress and wash’ may make great crested *Triturus cristatus* and smooth newts *Lissotriton vulgaris* palatable for grey herons *Ardea cinerea*, with a link to video evidence. *Herpetological Bulletin* **170**, 33–34 (2024).

35. S. H. Hurlbert, Predator Responses to the Vermilion-Spotted Newt (*Notophthalmus viridescens*). *Journal of Herpetology* **4**, 47–55 (1970).
36. C. G. Halpin, J. Skelhorn, C. Rowe, Increased predation of nutrient-enriched aposematic prey. *Proceedings of the Royal Society B: Biological Sciences* **281** (2014).
37. T. Carle, C. Rowe, Avian predators change their foraging strategy on defended prey when undefended prey are hard to find. *Animal Behaviour* **93**, 97–103 (2014).
38. T. G. Aubier, T. N. Sherratt, State-Dependent Decision-Making by Predators and Its Consequences for Mimicry. *The American Naturalist* **196**, E127–E144 (2020).
39. J. Skelhorn, C. Rowe, Predators' Toxin Burdens Influence Their Strategic Decisions to Eat Toxic Prey. *Current Biology* **17**, 1479–1483 (2007).
40. E. Alonso, A. Alfonso, M. R. Vieytes, L. M. Botana, Evaluation of toxicity equivalent factors of paralytic shellfish poisoning toxins in seven human sodium channels types by an automated high throughput electrophysiology system. *Archives of Toxicology* **90**, 479–488 (2016).
41. S. Zakrzewska, S. A. Nixon, Z. Chen, H. S. Hajare, E. R. Park, J. V. Mulcahy, K. M. Arlinghaus, E. Neu, K. Konovalov, D. Provasi, T. A. Leighfield, M. Filizola, J. Du Bois, D. L. Minor, Structural basis for saxitoxin congener binding and neutralization by anuran saxiphilins. *Nature Communications* **16**, 3885 (2025).
42. T. Vandendriessche, Y. Abdel-Mottaleb, C. Maertens, E. Cuypers, A. Sudau, U. Nubbemeyer, D. Mebs, J. Tytgat, Modulation of voltage-gated Na<sup>+</sup> and K<sup>+</sup> channels by pumiliotoxin 251D: A “joint venture” alkaloid from arthropods and amphibians. *Toxicon* **51**, 334–344 (2008).
43. Y. Wei, H. Mao, Q. Liu, W. Fang, T. Zhang, Y. Xu, W. Zhang, B. Chen, Y. Zheng, X. Hu, Lipid metabolism and microbial regulation analyses provide insights into the energy-saving strategies of hibernating snakes. *Communications Biology* **8**, 1–13 (2025).
44. A. Alvarez-Buylla, M.-T. Fischer, M. D. Moya Garzon, A. E. Rangel, E. E. Tapia, J. T. Tanzo, H. T. Soh, L. A. Coloma, J. Z. Long, L. A. O'Connell, Binding and sequestration of poison frog alkaloids by a plasma globulin. *eLife* **12**, e85096 (2023).
45. K. Barabas, W. P. Faulk, Transferrin receptors associate with drug resistance in cancer cells. *Biochemical and Biophysical Research Communications* **197**, 702–708 (1993).
46. S. Tortorella, T. C. Karagiannis, Transferrin Receptor-Mediated Endocytosis: A Useful Target for Cancer Therapy. *The Journal of Membrane Biology* **247**, 291–307 (2014).
47. L. Ruiz-Mazón, G. Ramírez-Rico, M. de la Garza, Lactoferrin: a secret weapon in the war against pathogenic bacteria. *Exploration of Drug Science* **2**, 734–743 (2024).
48. S. K. Nigam, What do drug transporters really do? *Nature Reviews Drug Discovery* **14**, 29–44 (2015).

49. M. D. Pizzagalli, A. Bensimon, G. Superti-Furga, A guide to plasma membrane solute carrier proteins. *The FEBS Journal* **288**, 2784–2835 (2021).
50. A.-M. Enge, F. Kaltner, C. Gottschalk, A. Braeuning, S. Hessel-Pras, Active Transport of Hepatotoxic Pyrrolizidine Alkaloids in HepaRG Cells. *International Journal of Molecular Sciences* **22**, 3821 (2021).
51. J. Waizenegger, J. Glück, M. Henricsson, C. Luckert, A. Braeuning, S. Hessel-Pras, Pyrrolizidine Alkaloids Disturb Bile Acid Homeostasis in the Human Hepatoma Cell Line HepaRG. *Foods* **10**, 161 (2021).
52. K. Kawai, R. Negoro, M. Ichikawa, T. Yamashita, S. Deguchi, K. Harada, K. Hirata, K. Takayama, H. Mizuguchi, Establishment of SLC15A1/PEPT1-Knockout Human-Induced Pluripotent Stem Cell Line for Intestinal Drug Absorption Studies. *Molecular Therapy Methods & Clinical Development* **17**, 49–57 (2020).
53. Y.-F. Han, X.-H. Fan, X.-J. Wang, K. Sun, H. Xue, W.-J. Li, Y.-B. Wang, J.-Z. Chen, Y.-S. Zhen, W.-L. Zhang, X. Zhou, R. Hui, Association of intergenic polymorphism of organic anion transporter 1 and 3 genes with hypertension and blood pressure response to hydrochlorothiazide. *American Journal of Hypertension* **24**, 340–346 (2011).
54. K. Engström, S. Ameer, L. Bernaudat, G. Drasch, J. Baeuml, S. Skerfving, S. Bose-O'Reilly, K. Broberg, Polymorphisms in genes encoding potential mercury transporters and urine mercury concentrations in populations exposed to mercury vapor from gold mining. *Environmental Health Perspectives* **121**, 85–91 (2013).
55. S. W. Yee, A. N. Nguyen, C. Brown, R. M. Savic, Y. Zhang, R. A. Castro, C. D. Cropp, J. H. Choi, D. Singh, H. Tahara, S. L. Stocker, Y. Huang, C. M. Brett, K. M. Giacomini, Reduced renal clearance of cefotaxime in asians with a low-frequency polymorphism of OAT3 (SLC22A8). *Journal of Pharmaceutical Sciences* **102**, 3451–3457 (2013).
56. F. Peelman, C. Labeur, B. Vanloo, S. Roosbeek, C. Devaud, N. Duverger, P. Denèfle, M. Rosier, J. Vandekerckhove, M. Rosseneu, Characterization of the ABCA transporter subfamily: identification of prokaryotic and eukaryotic members, phylogeny and topology. *Journal of Molecular Biology* **325**, 259–274 (2003).
57. L. Jia, J. L. Betters, L. Yu, Niemann-Pick C1-Like 1 (NPC1L1) Protein in Intestinal and Hepatic Cholesterol Transport. *Annual Review of Physiology* **73**, 239–259 (2011).
58. M. T. Damiani, M. Pavarotti, N. Leiva, A. J. Lindsay, M. W. McCaffrey, M. I. Colombo, Rab Coupling Protein Associates with Phagosomes and Regulates Recycling from the Phagosomal Compartment. *Traffic* **5**, 785–797 (2004).
59. M. E. Feder, G. E. Hofmann, Heat-Shock Proteins, Molecular Chaperones, and the Stress Response: Evolutionary and Ecological Physiology. *Annual Review of Physiology* **61**, 243–282 (1999).
60. T. M. Vu, A.-N. Ishizu, J. C. Foo, X. R. Toh, F. Zhang, D. M. Whee, F. Torta, A. Cazenave-Gassiot, T. Matsumura, S. Kim, S.-A. E. S. Toh, T. Suda, D. L. Silver, M. R.

- Wenk, L. N. Nguyen, *Mfsd2b* is essential for the sphingosine-1-phosphate export in erythrocytes and platelets. *Nature* **550**, 524–528 (2017).
61. B. Spolaore, J. Fernández, B. Lomonte, M. L. Massimino, F. Tonello, Enzymatic labelling of snake venom phospholipase A2 toxins. *Toxicon* **170**, 99–107 (2019).
  62. Y. Li, Y. Jiang, Y. Zhang, N. Li, Q. Yin, L. Liu, X. Lv, Y. Liu, A. Li, B. Fang, J. Li, H. Ye, G. Yang, X. Cui, Y. Liu, Y. Qu, C. Li, J. Li, D. Li, Z. Gai, S. Wang, F. Zhan, M. Liang, Abnormal upregulation of cardiovascular disease biomarker PLA2G7 induced by proinflammatory macrophages in COVID-19 patients. *Science Reports* **11**, 6811 (2021).
  63. L. S. Candels, S. Becker, C. Trautwein, PLA2G7: a new player in shaping energy metabolism and lifespan. *Signal Transduction and Targeted Therapy* **7**, 1–2 (2022).
  64. T. N. U. Le, T. Q. Nguyen, P. Kalailingam, Y. T. K. Nguyen, V. K. Sukumar, C. K. H. Tan, F. Tukijan, L. Couty, Z. Hasan, I. Del Gaudio, M. R. Wenk, A. Cazenave-Gassiot, E. Camerer, L. N. Nguyen, *Mfsd2b* and *Spns2* are essential for maintenance of blood vessels during development and in anaphylactic shock. *Cell Reports* **40**, 111208 (2022).
  65. S. L. Geffeney, E. Fujimoto, E. D. Brodie, E. D. Brodie, P. C. Ruben, Evolutionary diversification of TTX-resistant sodium channels in a predator-prey interaction. *Nature* **434**, 759–763 (2005).
  66. W. A. Catterall, Structure and function of voltage-gated sodium channels at atomic resolution. *Experimental Physiology* **99**, 35–51 (2014).
  67. R. Marquez, D. Mejia-Vargas, P. Palacios-Rodriguez, V. Ramirez-Castaneda, A. Amezcua, A new species of Andinobates (Anura: Dendrobatidae) from the Urabá region of Colombia. *Zootaxa* **4290**, 531–546 (2017).
  68. R. D. Tarvin, C. M. Borghese, W. Sachs, J. C. Santos, Y. Lu, L. A. O’Connell, D. C. Cannatella, R. A. Harris, H. H. Zakon, Interacting amino acid replacements allow poison frogs to evolve epibatidine resistance. *Science* **357**, 1261–1266 (2017).
  69. F. Abderemane-Ali, N. D. Rossen, M. E. Kobiela, R. A. Craig, C. E. Garrison, Z. Chen, C. M. Collieran, L. A. O’Connell, J. D. Bois, J. P. Dumbacher, D. L. Minor, Evidence that toxin resistance in poison birds and frogs is not rooted in sodium channel mutations and may rely on “toxin sponge” proteins. *Journal of General Physiology* **153** (2021).
  70. S. Mohammadi, L. Yang, A. Harpak, S. Herrera-Álvarez, M. del P. Rodríguez-Ordoñez, J. Peng, K. Zhang, J. F. Storz, S. Dobler, A. J. Crawford, P. Andolfatto, Concerted evolution reveals co-adapted amino acid substitutions in Na<sup>+</sup>K<sup>+</sup>-ATPase of frogs that prey on toxic toads. *Current Biology* **31**, 2530-2538.e10 (2021).
  71. J. van Thiel, M. A. Khan, R. M. Wouters, R. J. Harris, N. R. Casewell, B. G. Fry, R. M. Kini, S. P. Mackessy, F. J. Vonk, W. Wüster, M. K. Richardson, Convergent evolution of toxin resistance in animals. *Biological Reviews* **97**, 1823–1843 (2022).

72. C. R. Feldman, E. D. Brodie, E. D. Brodie, M. E. Pfrender, Constraint shapes convergence in tetrodotoxin-resistant sodium channels of snakes. *Proceedings of the National Academy of Sciences* **109**, 4556–4561 (2012).
73. H. Terlau, S. H. Heinemann, W. Stühmer, M. Pusch, F. Conti, K. Imoto, S. Numa, Mapping the site of block by tetrodotoxin and saxitoxin of sodium channel II. *FEBS Letters* **293**, 93–96 (1991).
74. P. M. Vaelli, K. R. Theis, J. E. Williams, L. A. O’Connell, J. A. Foster, H. L. Eisthen, The skin microbiome facilitates adaptive tetrodotoxin production in poisonous newts. *eLife* **9**, e53898 (2020).
75. J. W. McGlothlin, J. P. Chuckalovcak, D. E. Janes, S. V. Edwards, C. R. Feldman, E. D. Brodie, M. E. Pfrender, Parallel evolution of tetrodotoxin resistance in three voltage-gated sodium channel genes in the garter snake *Thamnophis sirtalis*. *Molecular Biology and Evolution* **31**, 2836–2846 (2014).
76. R. E. del Carlo, J. S. Reimche, H. A. Moniz, M. T. J. Hague, S. R. Agarwal, E. D. B. Iii, E. D. B. Jr, N. Leblanc, C. R. Feldman, Coevolution with toxic prey produces functional trade-offs in sodium channels of predatory snakes. *eLife* **13** (2024).
77. C. R. Feldman, A. M. Durso, C. T. Hanifin, M. E. Pfrender, P. K. Ducey, A. N. Stokes, K. E. Barnett, E. D. Brodie, E. D. Brodie, Is there more than one way to skin a newt? Convergent toxin resistance in snakes is not due to a common genetic mechanism. *Heredity* **116**, 84–91 (2016).
78. V. G. Christensen, E. Khan, Freshwater neurotoxins and concerns for human, animal, and ecosystem health: A review of anatoxin-a and saxitoxin. *Science of The Total Environment* **736**, 139515 (2020).
79. K. C. Pearson, R. D. Tarvin, A review of chemical defense in harlequin toads (Bufonidae: Atelopus). *Toxicon: X* **13**, 100092 (2022).
80. A. M. Jeckel, R. A. Saporito, T. Grant, The relationship between poison frog chemical defenses and age, body size, and sex. *Frontiers in Zoology* **12**, 27 (2015).
81. A. M. Jeckel, S. Kocheff, R. A. Saporito, T. Grant, Geographically separated orange and blue populations of the Amazonian poison frog *Adelphobates galactonotus* (Anura, Dendrobatidae) do not differ in alkaloid composition or palatability. *Chemoecology* **29**, 225–234 (2019).
82. J. P. Lawrence, B. Rojas, A. Fouquet, J. Mappes, A. Blanchette, R. A. Saporito, R. J. Bosque, E. A. Courtois, B. P. Noonan, Weak warning signals can persist in the absence of gene flow. *Proceedings of the National Academy of Sciences* **116**, 19037–19045 (2019).
83. E. D. Brodie, M. S. Tumbarello, The Antipredator Functions of *Dendrobates auratus* (Amphibia, Anura, Dendrobatidae) Skin Secretion in Regard to a Snake Predator (*Thamnophis*). *Journal of Herpetology* **12**, 264 (1978).

84. B. L. Williams, C. T. Hanifin, E. D. Brodie, E. D. B. III, Tetrodotoxin affects survival probability of rough-skinned newts (*Taricha granulosa*) faced with TTX-resistant garter snake predators (*Thamnophis sirtalis*). *Chemoecology* **20**, 285–290 (2010).
85. S. Chen, Y. Zhou, Y. Chen, J. Gu, fastp: an ultra-fast all-in-one FASTQ preprocessor. *Bioinformatics* **34**, i884–i890 (2018).
86. S. Chen, Ultrafast one-pass FASTQ data preprocessing, quality control, and deduplication using fastp. *iMeta* **2**, e107 (2023).
87. D. Kim, B. Langmead, S. L. Salzberg, HISAT: a fast spliced aligner with low memory requirements. *Nat Methods* **12**, 357–360 (2015).
88. G. Pertea, M. Pertea, GFF Utilities: GffRead and GffCompare. F1000Research 9:304 [Preprint] (2020). <https://doi.org/10.12688/f1000research.23297.1>.
89. G. H. Putri, S. Anders, P. T. Pyl, J. E. Pimanda, F. Zanini, Analysing high-throughput sequencing data in Python with HTSeq 2.0. *Bioinformatics* **38**, 2943–2945 (2022).
90. M. I. Love, W. Huber, S. Anders, Moderated estimation of fold change and dispersion for RNA-seq data with DESeq2. *Genome Biology* **15**, 550 (2014).
91. A. Alexa, J. Rahnenfuhrer, *topGO: Enrichment Analysis for Gene Ontology* (2022).
92. L. E. Overman, P. J. Jessup, Synthetic applications of N-acylamino-1,3-dienes. An efficient stereospecific total synthesis of dl-pumiliotoxin C, and a general entry to cis-decahydroquinoline alkaloids. *Journal of the American Chemical Society* **100**, 5179–5185 (1978).
93. J. W. Daly, H. M. Garraffo, T. F. Spande, V. C. Clark, J. Ma, H. Ziffer, J. F. Cover, Evidence for an enantioselective pumiliotoxin 7-hydroxylase in dendrobatid poison frogs of the genus *Dendrobates*. *Proceedings of the National Academy of Sciences* **100**, 11092–11097 (2003).
94. T. Fukuyama, L. V. Dunkerton, M. Aratani, Y. Kishi, Synthetic studies on histrionicotoxins. II. Practical synthetic route to (+)-perhydro- and (+)-octahydrohistrionicotoxin. *Journal of Organic Chemistry* **40**, 2011–2012 (1975).
95. J. W. Daly, I. Karle, C. W. Myers, T. Tokuyama, J. A. Waters, B. Witkop, Histrionicotoxins: Roentgen-Ray Analysis of the Novel Allenic and Acetylenic Spiroalkaloids Isolated from a Colombian Frog, *Dendrobates histrionicus*. *Proceedings of the National Academy of Sciences* **68**, 1870–1875 (1971).
96. L. E. Llewellyn, J. Doyle, A. P. Negri, A high-throughput, microtiter plate assay for paralytic shellfish poisons using the saxitoxin-specific receptor, saxiphilin. *Analytical Biochemistry* **261**, 51–56 (1998).
97. S. F. Altschul, W. Gish, W. Miller, E. W. Myers, D. J. Lipman, Basic local alignment search tool. *Journal of Molecular Biology* **215**, 403–410 (1990).



98. OpenAI, ChatGPT (version GPT-5) (2025). <https://chat.openai.com>.

**Acknowledgments:** We are thankful for the opportunity to observe and interact with snakes and frogs, to witness them up close, and to share a home with them, the forest, and the cities where they live. We thank J. Du Bois for supplying STX samples. The Spanish translation was produced using ChatGPT and edited by VRC (Available in Data S5) (98). ChatGPT was also used to correct coding errors and to organize the pipelines.

**Funding:**

National Institutes of Health R35GM150574 (RDT)

National Institutes of Health 1S10GM154292-01 (RWF)

National Science Foundation DUE-0942345 and IOS-1556982 (RWF)

Russell E. Train Education for Nature Program (EF14103) from the World Wildlife Fund (VRC)

MVZ Wake Research Award, Museum of Vertebrate Zoology at UC Berkeley (VRC)

GRAC Research Funds, Integrative Biology Department at UC Berkeley (VRC)

Partially supported by grants from the Department of Defense HDTRA-1-19-0040, HDTRA-1-21-1-0011, and HDTRA-1-23-0026 (DLM)

**Author contributions:** Conceptualization: VRC, RDT

Data curation: VRC, SAN, DAN, RWF

Formal analysis: VRC, SAN, RWF, DAN

Funding acquisition: VRC, RDT, DLM, RWF

Investigation: VRC, SAN, DAN, RWF, DLM

Methodology: VRC, SAN, DSV, DAN, RDT

Project administration: VRC, DLM, RDT

Resources: DAN, DLM, RDT, RWF, DSV

Software: VRC, SAN, RWF

Supervision: VRC, FA, DLM, RDT

Validation: FA, DLM, RDT

Visualization: VRC, SAN, DLM

Writing - original draft: VRC, SAN, RDT, DLM, RWF

Writing - review & editing: VRC, SAN, DAN, DSV, FA, RWF, DLM, RDT

**Diversity, equity, ethics, and inclusion [optional]:** Thanks to José Rances Caicedo Portilla, Martha Calderón and Kannon Pearson for all your help during the animal collection process.

We are very grateful to all the members of the Minor Lab and the Tarvin Lab for their help during the electrophysiology experiments, and to the EGL Laboratory and QB3 Genomics, especially Lydia Smith and Sophie Draper, for your dedicated support during the transcriptome library preparation. Special thanks to José Guillermo Díaz Cahuachi, Ana Milena Castro, Francly Silva, the Kuiru family (Mirna Kuiru, Luna, Marco, and Camila), and the Naforo-Bautista family (Maritza Naforo Bautista, María Bautista Pinto, Juan Naforo Bautista, Orfilia Gomez, Velentina) for your knowledge, kindness, and invaluable help during sample collection, predation experiments, and in general, for making this research possible. We thank Reserva Maiku in Puerto Nariño and the Hermanos Menores Capuchinos de Leticia for granting us permission to work on their lands. We are deeply grateful to all the local guides and workers who assisted us and generously shared their time and knowledge.

**Competing interests:** Authors declare that they have no competing interests.

**Data and materials availability:** Transcriptome raw data is available in Bioproject PRJNA1274516, see complete biosample numbers in table S1. Transcriptome code is available in [https://github.com/esperando370/Ereginae\\_transcriptome](https://github.com/esperando370/Ereginae_transcriptome). GC-MS data is available in MassIVE dataset (MSV000098843). Other data is available in the main text or the supplementary materials.

## Supplementary Materials

Materials and Methods

References (7, 15, 83-97)

Figs. S1 to S8

Tables S1 to S3

Movies S1 to S2

Data S1 to S8

Supplementary Materials for

**Toxin resistance mechanisms span biological scales in the Royal Ground Snake**  
*Erythrolamprus reginae*

V. Ramírez-Castañeda<sup>1\*</sup>, S. A. Nixon<sup>2</sup>, D Alarcón-Naforo<sup>3</sup>, F. Abderemane-Ali<sup>4</sup>, R. W. Fitch<sup>5</sup>,  
D. Salazar-Valenzuela<sup>6</sup>, D. L. Minor, Jr.<sup>2,7,8,9,10</sup>, R. D. Tarvin<sup>1\*</sup>

Corresponding author: [vramirez@berkeley.edu](mailto:vramirez@berkeley.edu), [rdtarvin@berkeley.edu](mailto:rdtarvin@berkeley.edu)

**The PDF file includes:**

Materials and Methods  
Figs. S1 to S8  
Tables S1 to S3  
References

**Other Supplementary Materials for this manuscript include the following:**

Movies S1 to S2  
Data S1 to S8

## Materials and Methods

### Animal collection

We collected 12 *Erythrolamprus reginae* snakes, 6 *Ameerega trivittata* frogs, and 6 *Scinax ruber* frogs from Leticia, Amazonas, Colombia (Table S1). These specimens were captured by hand or using a snake hook. Collection permit was granted by the Colombian Authority for Environmental Licenses (ANLA; No. 1249, 23 July 2020, RCI0002-00-2020). To avoid any impact of chemical euthanasia on our results, we euthanized snakes by decapitation followed by rapid extraction of the brain tissue. Frogs were euthanized using hypothermic shock. Euthanasia and predation trial (below) protocols were approved by the IACUC No. AUP-2019-08-12457-1 issued by the University of California Berkeley, USA. Non-CITES tissue samples were exported under the ANLA permits No. 02191, No. 02376, and No. 3271. For *A. trivittata* the exportation of the tissues was granted by the CITES export permits No. CO26165 and No. CO46959.

### Predation Behavior Test

We hand or snake-hook captured snakes and housed them individually close to the site of capture in mesh cages (30 cm x 30 cm from RestCloud) with water, and natural leaves, ground, and hiding spots (log cylinders) for an acclimatization period of five days. This period ensured that the digestive tracts of the snakes were empty before the experiment. The anurans were collected one or two days before each trial and kept under the same mesh cages conditions. We video-recorded using a Nikon D5600 camera *E. reginae* predation events against the poisonous frog *A. trivittata* (Dendrobatidae) and the non-poisonous *S. ruber* (Hylidae; Dataset S1 & Dataset S2). If after 2 hours the toxic frog was not ingested, we removed the toxic frog, and a second frog—*Leptodactylus* sp., *Sphaenorynchus lacteus*, *Dendropsophus* sp., *Rhinella margaritifera*, or *Scinax ruber*—was introduced to the enclosure to determine whether the snake was generally unwilling to eat or specifically rejected *A. trivittata* (see Fig. 1A). All offered frogs are natural prey of *E. reginae*, ensuring that the experiment simulated natural feeding conditions.

During the experiment, the snake and posteriorly the frog were introduced into an empty mesh enclosure. We recorded the interaction until 40 minutes after ingestion or vomiting of the frog, or up to two hours if no ingestion occurred. If no predation was observed, the trial was terminated after two hours. Predation events were classified as "ingested," "vomited," or "avoided" following Brodie and Tumbarello (83). Snakes were euthanized 40 minutes after the frog was completely swallowed to obtain tissue samples for transcriptome analysis. According to Williams et al. (84), toxin intoxication effects become measurable within 30–40 minutes post-ingestion. Video recordings were analyzed to document notable behaviors, including the time elapsed from the first attack to the moment the frog was fully swallowed ("Time to swallow") and the number of times the snake exhibited dragging behavior ("Dragging cycles"). We define dragging behavior as the act of swabbing or rubbing the frog, already held in the snake's mouth, along the floor or wall. Each dragging cycle was counted from the moment the snake began dragging to when it paused, rather than based on the number of physical drags performed.

### Transcriptome

#### *RNA library preparation*

Snakes were sacrificed after each predation experiment (*A. trivittata* or *S. ruber* ingestion) or after a 5-day fasting period (control; Table S2). Snake tissues were collected in the field, stored in RNA later, and transported for a longer storage at -80 °C freezer (Table S2). For RNA extraction, we used the Monarch® Total RNA Miniprep Kit from NEB Biolab and followed the protocol for <10 mg initial tissue. The homogenization of the tissues was performed using the PowerLyzer™ 24 bead beater (MO BIO Laboratories, Inc.), with two cycles of 3500 RPM for 45 seconds, each followed by a 30-second rest period, and an intermediate speed of 3500 RPM. To assess starting RNA quantity and quality, we used the Qubit RNA HS Assay Kit from ThermoFisher Scientific and Bioanalyzer RNA Analysis from Agilent.

For the RNA library prep, we selected the high quality RNA samples (RIN  $\geq$  7) with up to 500 ng RNA, except for a few irreplaceable samples that had low RIN scores despite several extraction attempts. We followed a poly(A) selection protocol for all samples using the Watchmaker mRNA Capture Kit from Watchmaker Genomics. For the library amplification, seven extra cycles were used for the low RIN score samples (Table S2). RNA libraries were sequenced to obtain ~30 M paired-end reads (150 bp) per tissue on a Illumina NovaSeq™ X 10B flow cell. Raw data is available in (Bioproject PRJNA1274516, see complete biosample numbers in table S1).

#### *RNA-seq data processing and analysis*

Raw paired-end RNA-seq reads were quality-filtered and trimmed using fastp v0.23.2 (85, 86) with adapter detection enabled and default settings. Cleaned reads were aligned to the *E. reginae* reference genome (GCF\_031021105.1) using HISAT2 v2.2.1 (87) with the *--dta* flag to facilitate transcript assembly. Alignment outputs in SAM format were converted to BAM, sorted, and indexed using Picard and samtools v1.21. Alignment quality metrics were generated with the *flagstat* tool. The genome annotation file (GFF) was converted to GTF format using *gffread* (88), with manual correction of gene identifiers to ensure compatibility with downstream quantification tools. Transcript abundance was quantified using HTSeq-count v0.13.5 (89) in unstranded mode (-s no) with exon-level features and gene-level aggregation (-i gene\_id).

Transcript abundance data were analyzed using DESeq2 in R (v4.3.0) (90). Count matrices from HTSeq-count were merged and filtered to include genes expressed in digestive tissues: liver, tongue, stomach, and intestine. These tissues were obtained from 3 different feeding treatments (see above): after 5 days fasting, or 40 minutes after the ingestion of an *A. trivittata* or *S. ruber* prey. Differential gene expression (DE) analyses were performed using DESeq2 with tissue and condition as covariates (see dataset S3: log2fold and p-value results). Principal component analysis (PCA) and volcano plots were generated to assess sample clustering and DE genes (Fig. S7). Genes with adjusted p-value < 0.05 and log2FoldChange > 0 were considered significant and upregulated (Dataset S3). The final list of upregulated genes for each condition was compiled by combining DE genes identified across the three pairwise comparisons: fasting vs. *A. trivittata*, fasting vs. *S. ruber*, and *S. ruber* vs. *A. trivittata*. For the expressed gene counts, we retained only protein-coding genes from the set of upregulated transcripts by filtering the set of upregulated genes by *E. reginae* gene identifiers from the NCBI genome annotation classified as protein-coding. To investigate functional patterns of gene expression across conditions, we classified differentially expressed genes into biologically relevant categories based on gene name

patterns and annotations. Using regular expressions, we extracted gene sets associated with specific protein families and functional categories from the differential expression results.

Gene categories related to toxin resistance were used to highlight potential differential expression of these genes in the volcano plots (Fig. S7). We grouped solute carrier family genes (SLC), phospholipase A2 genes (PLA2), cytochrome P450 genes (CYP), serine protease inhibitors (SERPIN), ATP-binding cassette transporters (ABC), heat shock proteins (HSP), and Rab GTPases (RAB) based on their gene name prefixes. Transferrin-related genes (TF, TFRC, TFIP11, and TFR2) were grouped using known gene symbols. Cholinesterase-like genes (*E. reginae* transcript IDs: LOC139158370–LOC139158371, LOC139159376, LOC139160160, LOC139160166, LOC139160209–LOC139160211, LOC139160214–LOC139160215, LOC139160217, LOC139160219–LOC139160220, LOC139160232), lactotransferrin-like gene (ID: LOC139173594 and LTF) and 85 transporters genes (Data S8) were manually identified using the ncbi gene annotations of *Erythrolamprus reginae* (GCF\_031021105.1).

Functional enrichment of DE genes was assessed using topGO (ontology: Molecular Function) (91). Gene-to-GO mappings were obtained using *Anolis carolinensis* annotations (Unitprot taxon ID 28377). Only genes with detectable expression across samples (mean normalized counts > 0.5) were used as background. Enrichment results were visualized using the molecular function option “MF” and cellular component option “CC”.

#### Skin secretion GC-MS toxin profile analysis

Following euthanasia, we removed entire skins from 6 *A. trivittata* and 6 *S. ruber* and placed each in ~1 mL 100% ethanol in glass vials with PTFE-lined caps and stored at -80 °C. A 100 µL aliquot of the solution was sampled and analyzed directly by Gas-Chromatography Mass-Spectrometry (GC-MS). Samples (1 µL) were analyzed using either a Thermo iTQ1100 unit resolution ion trap instrument or Thermo Exploris GC high-resolution orbitrap instrument. GC separation used 5% phenyl methylsilicone columns (Restek RTX-5MS or Thermo TG-5Si, 0.25 mm x 30m, 0.25 µm film thickness) with splitless injection with a ramp from 100C to 280C as previously described. Retention indices (Kovats) were determined by comparison to alkane standards injected with the group. Samples were sequentially analyzed in electron ionization (EI) and chemical ionization with ammonia reagent gas (CI-NH<sub>3</sub>). Compounds were identified by comparison with EI library spectra, molecular weight/formula match, and retention index.

#### Toxin sources and preparation for electrophysiology analyses

STX was synthesized as described (Andresen and Bois 2009). Neosaxitoxin (neoSTX) was purchased from Sigma Aldrich (Sigma-Aldrich GmbH, Switzerland, cat. no. 41619). Tetrodotoxin citrate (TTX) was purchased from Cayman Chemical (MI, USA, cat. no. NC1735928). All toxins were lyophilized and dissolved in ultrapure water in stocks of 1–5 mM for further use.

From the original 100% ethanol solution containing whole-skin extracts of *A. trivittata* and *S. ruber*, 100 µl was taken from each individual skin sample to create a combined 600 µl skin secretion solution for each species. Ethanol was evaporated using a low-pressure nitrogen flow in

a Rotavapor R-300 vacuum system (100 mbar, 35 °C). The resulting solute was then resuspended in 30  $\mu$ l of ultrapure water containing 5% DMSO to facilitate the dilution of hydrophobic compounds.

Another five toxins found in dendrobatid frogs were shared by the Fitch lab (coauthor) from the John W. Daly laboratory collection (4). Decahydroquinoline **195A** (DHQ **195A**, aka PTX-C, PTX-C<sub>I</sub>), Synthetic racemic DHQ **167** HCl, (aka PTX-C<sub>IV</sub>) was a generous gift of Dr. Larry Overman (92). Synthetic (+)-PTX **251D** HCl was prepared as described (93). Racemic octahydrohistrionicotoxin HCl (H8-HTX, HTX **291A**) was a generous gift of Dr. Yoshito Kishi (94). Natural Histrionicotoxin (HTX **283A**) was isolated from mixed frog collections (95). were diluted in ultrapure water or ultrapure water plus 5% DMSO to obtain a 30nM to 100 nM stock dilution (Table S3).

### Generating liver soluble protein extracts

*E. reginae* ( $n = 2$ ) and *C. tenuis* ( $n = 1$ ) specimens were collected and euthanized according to approved UCB IACUC protocols (AUP-2019-08-12457) and a California Department of Fish and Wildlife Scientific Collecting Permit S-190980001-19111-001 (Table S1). Animals were humanely euthanized via decapitation, and liver samples were immediately dissected, flash-frozen, and stored at -80°C. Control mouse liver samples were collected from 5–6-week-old female CD1-IGS mice (Charles River Laboratories, Wilmington, MA, USA) under UCSF IACUC protocol AN076215-01F, and immediately flash-frozen in liquid nitrogen and stored at -80°C. Liver homogenization was adapted from descriptions of isolating soluble toxin-binding proteins from animal tissues by Llewellyn *et al.* (15, 96) and 1998. In brief, livers were homogenized at approximately 1 ml per g of tissue in a buffer consisting of 10 mM Tris-HCl, 0.2 mM ethylenediaminetetraacetic acid (EDTA), pH 7.4, supplemented with EDTA-free protease inhibitor tablets (ThermoFisher Scientific, Waltham, MA, USA, Cat. A32955). Livers were homogenized using a PowerLyzer™ 24 bead beater with two cycles of 3500 rpm for 45 seconds, 30 seconds rest, and 3500 rpm for 45 seconds. Liver extracts were then centrifuged at 10,000 g for 15 minutes and the resultant pellet was discarded. The supernatant was filtered and then flash-frozen and stored at -80°C until use. Total protein was measured using the Pierce bicinchoninic acid (BCA) protein assay (ThermoFisher Scientific, cat. no. 23225) and extracts standardized to 0.2 mg/mL final concentration.

### Mammalian cell culture

Chinese hamster ovary (CHO) cells stably expressing the  $\alpha$ -subunit of the human skeletal muscle sodium channel isoform (*HsNa<sub>v</sub>1.4*, NM\_00334.4, B'SYS GmbH, cat. no. BSYS-NaV1.4-CHO-C) were maintained at 37°C, 5% CO<sub>2</sub> in culture medium containing Ham's F-12 medium with GlutaMAX (Gibco, cat. no. 31765035) supplemented with 9% (v/v) heat-inactivated fetal bovine serum (Gibco, cat. no. 16140071), penicillin-streptomycin (0.9% (v/v), Gibco, cat. no. 15-140-122) and 100  $\mu$ g/mL Hygromycin B (Sigma-Aldrich, cat. no. 10843555001).

### Whole-cell patch-clamp electrophysiology

The effects of treating toxins with liver extract on *HsNa<sub>v</sub>1.4* were assessed using a semi-automated QPatch Compact II electrophysiology platform (Sophion Bioscience, Ballerup, Denmark). Recordings were conducted at 22°C. The intracellular solution (IC) contained the following in mM: 140 CsF, 1/5 EGTA/CsOH, 10 HEPES, 10 NaCl (pH 7.3 with 3M CsOH), 320 mOsm. The extracellular solution (EC, saline) contained the following in mM: 2 CaCl<sub>2</sub>, 1 MgCl<sub>2</sub>, 4 KCl, 145 NaCl, 10 HEPES, 10 glucose (pH 7.4 with NaOH), 305 mOsm. Solutions were filtered using a 0.22 μM membrane filter.

Before recording, cells were washed with Dulbecco's phosphate buffered saline (DPBS, Gibco, cat. no. 14190144), detached from culture flasks with Detachin (AMSBIO, cat. no. T100100) and then kept in serum-free medium (Sigma-Aldrich, cat. no. C5467) supplemented with 25 mM HEPES and 0.04 mg/mL soybean trypsin inhibitor (Sigma-Aldrich, cat. no. 10109886001). Immediately prior to recording, cells were washed and resuspended in EC to a final cell density of 4–6 x 10 cells/mL, and then applied to the QPatch Compact II (Sophion Bioscience, Ballerup, Denmark) using 8-channel QPlate 8X multihole chips (Sophion Bioscience, cat. no. SB0210).

Sodium currents were acquired at 25 kHz and filtered at 8333 kHz, with leak subtraction protocol applied and non-leak subtracted currents acquired in parallel. Sodium currents were elicited using a single pulse protocol where cells were held at -90 mV, with a hyperpolarization step of -120 mV for 200 ms followed by a depolarization step to 0 mV for 60 ms and then returned to a holding potential of -90 mV, with sweep-to-sweep interval duration of 10 seconds. All recordings were conducted at 22°C.

The effect of guanidinium toxins alone on *HsNa<sub>v</sub>1.4* in CHO cells were first assessed by determining cumulative toxin concentration-response curves, with toxin solutions prepared in 3-fold serial dilution series in EC and applied as increasing concentrations. The IC<sub>50</sub> concentrations were calculated by fitting the concentration-response curves with non-linear regression models in GraphPad Prism V10.0. Toxin concentrations sufficient to block ~90% of *HsNa<sub>v</sub>1.4* currents were subsequently calculated using the IC<sub>50</sub> and hillslope (*H*) as follows:

$$IC_x = \left( \frac{x}{100-x} \right)^{\frac{1}{H}} \times IC_{50}$$

The effect of incubating toxin in liver extract was assessed by diluting samples in EC containing 0.05% w/v bovine serum albumin (BSA) and then incubating at room temperature (23 ± 2°C) for 30 min. Samples included: toxin alone; toxin combined with liver extract (0.2 mg/mL final); and liver extract alone (0.2 mg/mL). Where possible, toxin concentrations were selected with the aim of inhibiting 90% of sodium currents, which were calculated from the toxin concentration-response curves to be approximately 1.5 nM for neoSTX, 100 nM for STX, and 300 nM for TTX. In the case of frog-derived alkaloids, where toxin quantities were exceedingly limited, a single high concentration able to block putatively resistant *Erythrolamprus reginae* *ErNa<sub>v</sub>1.4* by at least 60% was selected: 250 μM H<sub>8</sub>-HTX; 500 μM HTX283A; 500 μM PTX251D; and *A. trivittatta* skin extract (1:200 dilution). After incubating, these samples were applied to *HsNa<sub>v</sub>1.4* cells, in stable whole-cell patch-clamp configuration with minimum of 1 nA of sodium current, in a successive fashion. First, steady baseline sodium currents were established in EC, followed by inhibiting currents with toxin-alone. Toxin samples were then washed out until currents returned to baseline, using at least nine chamber volumes of EC. The



toxin:liver extract mix was then applied and compared against currents elicited in EC and toxin alone solutions. Finally, the toxin:liver extract mix was washed out and then liver extract alone was applied as a control. See Fig. S3 for schematic of assay. All liver extracts and toxins were screened at minimum in duplicate in two independent assays. Normalized current recovery was then determined using the following equation:  $\frac{I_{\text{toxin:liver}} - I_{\text{toxin}}}{I_{\text{control}}}$ , where  $I_{\text{control}}$  is the baseline current elicited in EC,  $I_{\text{toxin}}$  is the current after application of toxin alone, and  $I_{\text{toxin:liver}}$  is the current following application of the mixed toxin:liver extract. The degree of current recovery for each toxin between different species of liver extract was compared by one-way ANOVA with Tukey's post hoc test. All data analyses were performed using Sophion Analyzer software (Sophion Bioscience) and GraphPad Prism v10.0 (GraphPad Prism, San Diego, CA, USA).

### Gene Reconstruction and Cloning of *E. reginae* Na<sub>v</sub>1.4 (NR & R) and HsNa<sub>v</sub>1.4

We used the *E. reginae* complete Na<sub>v</sub>1.4 gene reconstruction from sample No. GECO H 2823 collected in Santa María, Boyacá, Colombia, with complete information published in Ramírez-Castañeda et al. (7), as the template. Minor gaps in the sequence were completed using transcriptome samples generated in this study, employing BLAST v2.7.1+ to identify the required sites (97).

Gene synthesis and cloning into the pcDNA3.1+ vector were requested from GenScript USA Inc. for two sequences: a non-resistant variant and a resistant variant of the *E. reginae* Na<sub>v</sub>1.4 channel, following the sequences published in Ramírez-Castañeda et al. (7) (*Er*Na<sub>v</sub>1.4-NR and *Er*Na<sub>v</sub>1.4-R) (see Fig. S1 & complete sequences in Dataset S4). Additionally, we ordered the complete synthesis and cloning of the human Na<sub>v</sub>1.4 channel into pcDNA3.1 from the same company (Ref=CCDS:CCDS45761.1, protein\_id=NP\_000325.4) (*Hs*Na<sub>v</sub>1.4; GenScript USA Inc.) (complete sequences in Dataset S4). Nomenclature to highlight amino-acid homologous positions is based on the human Na<sub>v</sub>1.4 sequence.

In initial trials, the *Er*Na<sub>v</sub>1.4 (NR) and *Er*Na<sub>v</sub>1.4 (R) constructs were found to be unstable during replication. To address this, we used CopyCutter™ EPI400 Chemically Competent *E. coli* cells from VWR International and followed the recommended protocol.

### Two-electrode voltage-clamp electrophysiology (TEVC)

Two-electrode voltage-clamp (TEVC) recordings were conducted using defolliculated *Xenopus laevis* oocytes at developmental stages V–VI. Oocytes were harvested following UCSF IACUC protocol AN178461, with recordings performed 1–2 days after microinjection with *Hs*Na<sub>v</sub>1.4 mRNA and 3–4 days post-injection for *E. reginae* Na<sub>v</sub>1.4 (NR & R). Linearized cDNA constructs were transcribed into capped mRNA using the mMACHINE T7 Transcription Kit (Invitrogen). Microinjections were performed using 9–16 ng of *Hs*Na<sub>v</sub>1.4 mRNA and 50–64 ng of *E. reginae* Na<sub>v</sub>1.4 (NR & R) mRNA. Data acquisition was carried out using a GeneClamp 500B amplifier (MDS Analytical Technologies) controlled by pClamp software (Molecular Devices), with signals digitized at 1 kHz using a Digidata 1332A digitizer (MDS Analytical Technologies). Oocytes were impaled with borosilicate glass microelectrodes

(0.3–3.0 MΩ resistance) filled with 3 M KCl. Sodium currents were recorded in a bath solution (RS) composed of 96 mM NaCl, 1 mM CaCl<sub>2</sub>, 1 mM MgCl<sub>2</sub>, 2 mM KCl, and 5 mM HEPES (pH 7.5, adjusted with NaOH).

To determine the concentration–response relationship for STX, TTX, and neoSTX, test solutions containing specific toxin concentrations were sequentially applied via perfusion to oocytes expressing the channels ( $n = 6$  oocytes, per Na<sub>v</sub> channel and toxin). Sodium currents were elicited using a single-pulse protocol where oocytes were held at -120 mV for 3 s, followed by a depolarization step to 0 mV for 60 ms, before returning to -120 mV. The interval between sweeps was 10 s.

For STX and TTX, toxin block was washed out between concentrations (approximately 20 sweeps). For neoSTX, a cumulative toxin recording approach was used, where each concentration was maintained for ~50 sweeps. The IC<sub>50</sub> values (Fig. 2 and Table S4), representing the toxin concentration required to inhibit 50% of the current, were calculated by fitting concentration-response curves based on the ratio of peak currents in the presence and absence of toxin using the equation:

$$I_x = (I_{max} - I_{min}) / (1 + IC_x / IC_{50})$$

where  $I_x$  represents the current amplitude at toxin concentration  $x$ ,  $I_0$  is the current amplitude in the absence of toxin, and  $I_{max}$  and  $I_{min}$  correspond to the maximum and minimum peak current amplitudes, respectively.

Due to the limited availability of skin secretions and other dendrobatid toxins, a single toxin concentration was applied to the TEVC chamber for single-pulse recordings, followed by washout with buffer for ~50 sweeps ( $n = 3$  oocytes per Na<sub>v</sub> channel and toxin). The following toxin concentrations were used: a 1:100 dilution of *A. trivittata* and *S. ruber* skin extract, 500 μM H8-HTX, 500 μM HTX, 500 μM PTX251D, 1000 μM DHQ195A, and 1000 μM DHQ167. The available toxin quantities were insufficient to conduct tests with multiple concentrations. For statistical analysis, a non-parametric Mann-Whitney test was used to compare the reduction in current in the presence and absence of the toxin.

Activation and inactivation properties of each expressed Na<sub>v</sub> channel were determined using specific voltage protocols. Inactivation was measured by holding the membrane potential at -120 mV for 30 ms, followed by incremental 10 mV depolarization steps for 600 ms, ending with a final step to 0 mV for 30 ms before returning to -120 mV. Activation was assessed by first applying a hyperpolarization step to -100 mV for 6.5 ms, followed by a depolarization from -100 mV to 70 mV by incremental 5 mV depolarization steps for 60 ms before returning to -120 mV.

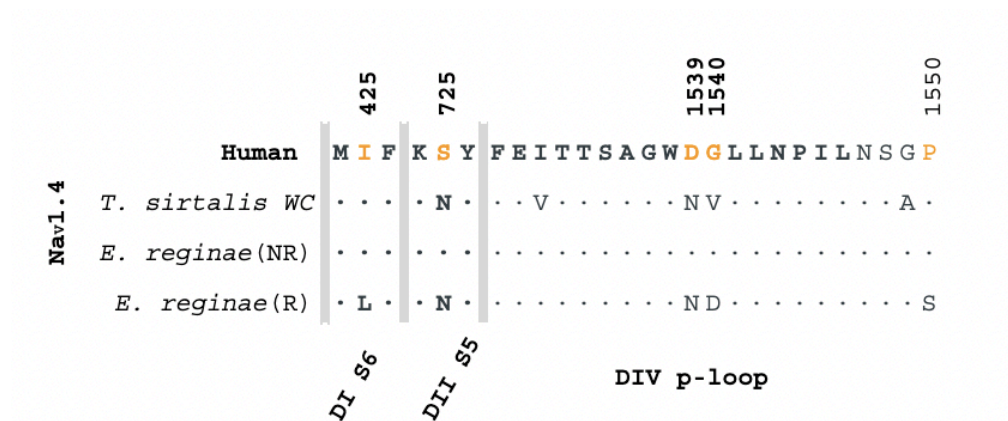


**Fig. S1.** The set of amino acid differences between *E. reginae* non-resistant and resistant Nav1.4 variants introduced the cloning vector.

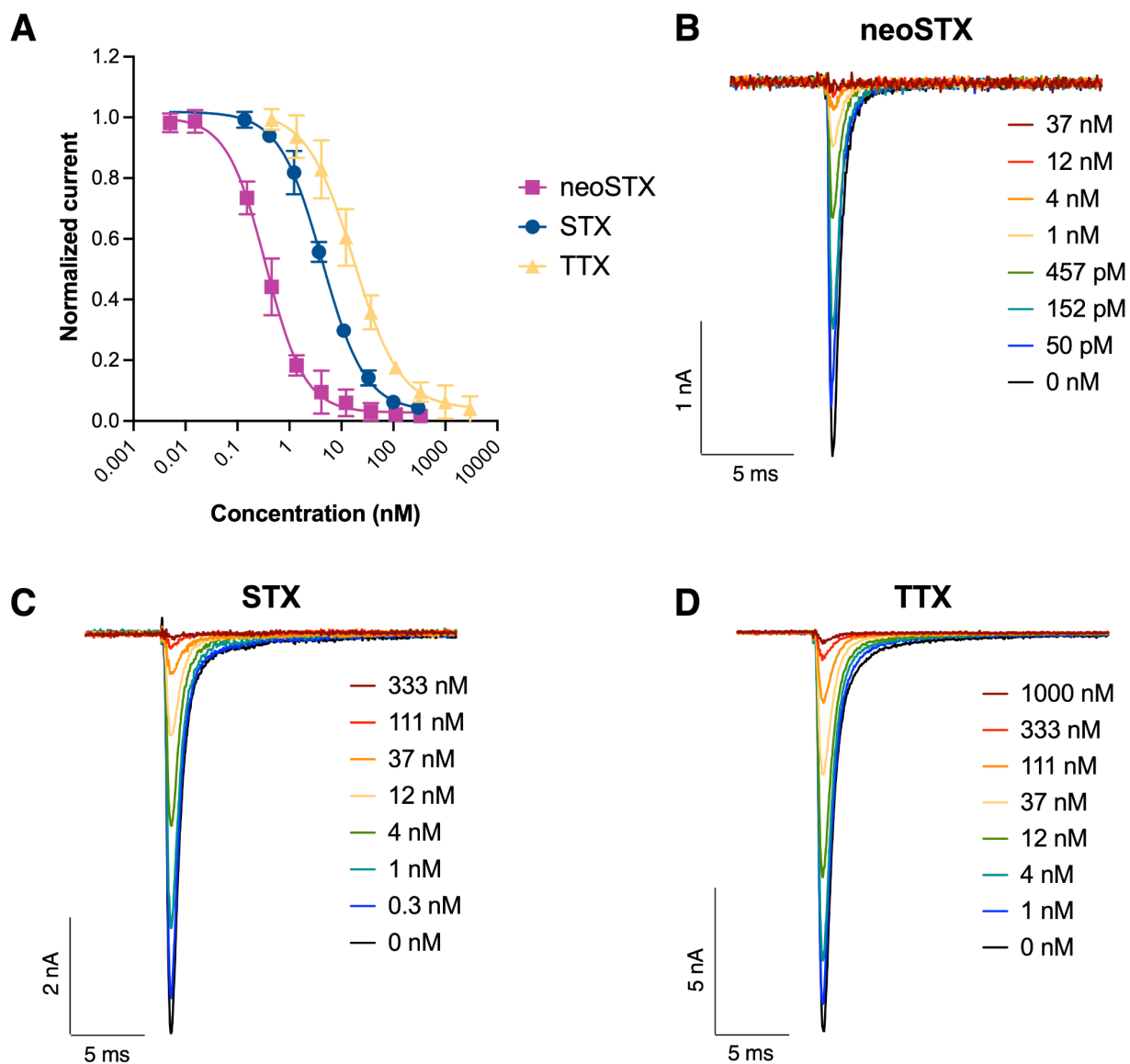


**Fig. S2. Whole-cell patch-clamp recordings of *HsNav1.4* responses to guanidinium toxins.** (A) Concentration-response curves to neoSTX (purple, squares), STX (blue, circles) and TTX (yellow, triangles). Each point represents the mean with standard deviation,  $n = 5-6$  cells. (B-D) Exemplar whole-cell patch-clamp recordings for increasing concentrations of toxins for neoSTX (B), STX (C), and TTX (D).

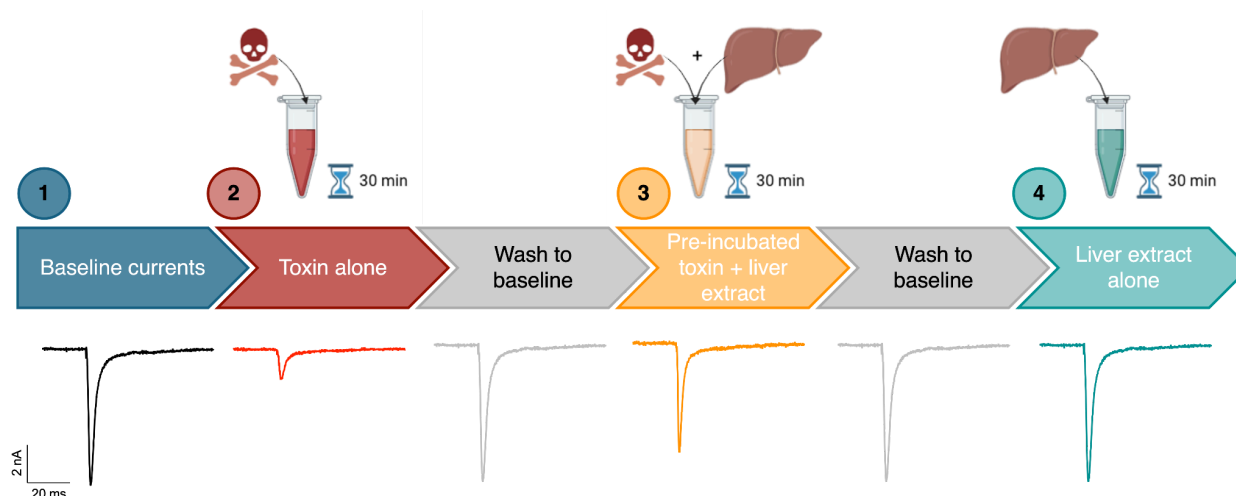


**Fig. S3. Schematic for liver extract functional toxin neutralization assay with example *HsNav*<sub>1.4</sub> currents.** The capacity for liver protein extracts from different organisms to inhibit the toxin block of *HsNav*<sub>1.4</sub> were measured by planar patch-clamp assay using a QPatch Compact II (Sophion Bioscience). Cells were sequentially exposed to four different conditions, with wash steps between: **1. Baseline currents** in ECS (blue), with no toxin or liver extract. **2. Toxin alone** (red), TTX, STX, neoSTX, PTX251D, H8-HTX, HTX283A, and *A. trivittata* skin secretion were diluted in ECS to concentrations sufficient to inhibit *HsNav*<sub>1.4</sub> currents by at least 60% and were pre-incubated for 30 minutes before addition to cells. **3. Toxin:liver extract mixture** (yellow), toxins from (2) were pre-incubated for 30 minutes at room temperature with liver extracts (final concentration 0.2 mg/mL) from *E. reginae*, *C. tenuis* (a control species of Colubrid snake from California, USA, with no known exposure to dendrobatid toxins), and mouse liver. If the toxin block observed in (2) was reduced in the presence of a liver extract, we inferred that the extract contained a detoxifying or toxin-binding protein. **4. Liver alone** (teal), liver extracts alone (final concentration 0.2 mg/mL) were incubated for 30 minutes at room temperature and added to the cells. If the liver extract alone affected sodium channel function, it would indicate intrinsic toxicity to *HsNav*<sub>1.4</sub>. Figure was partially generated using <https://Biorender.com>.

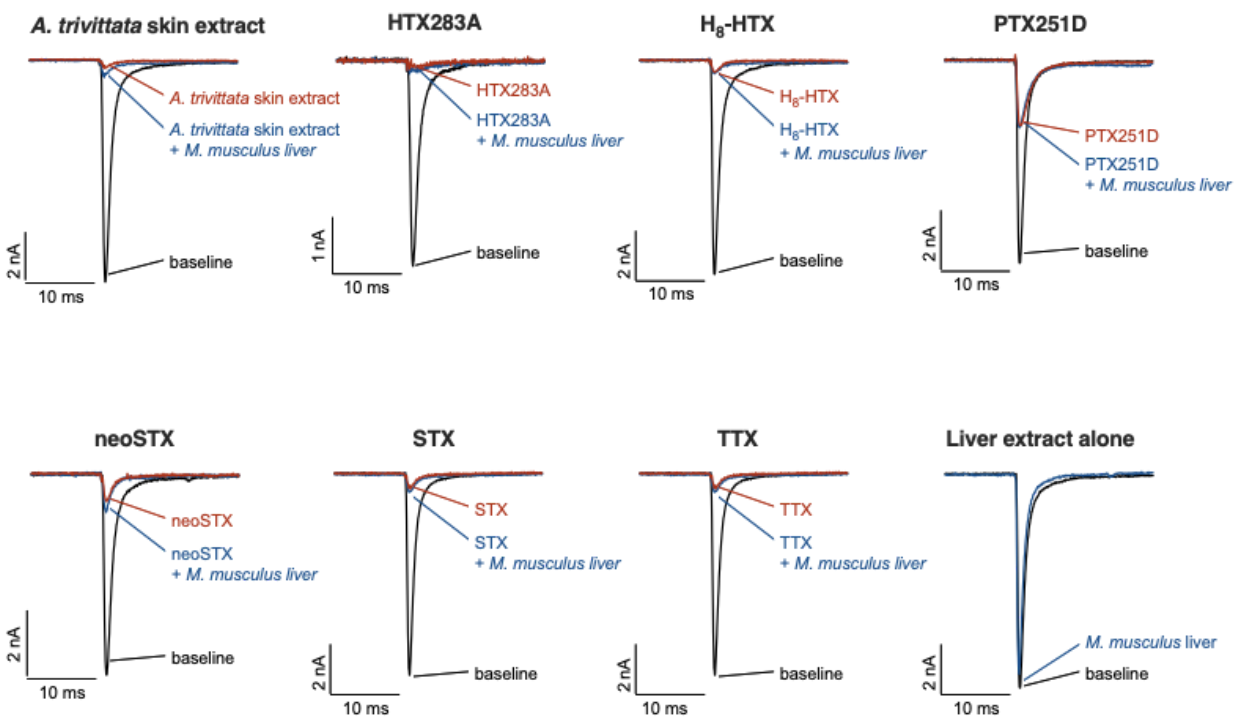


**Fig. S4. Mouse liver extract does not affect toxin block of *HsNaV1.4*.** Exemplar whole-cell patch-clamp recordings of *HsNaV1.4* expressed in CHO cells in the absence of toxin (baseline, black), presence of toxin alone (maroon) and toxin mixed with *M. musculus* liver extract (blue). Toxin concentrations used: *A. trivittata* skin extract diluted 1:200; HTX283A, 500  $\mu$ M; H<sub>8</sub>-HTX, 250  $\mu$ M; PTX251D, 500  $\mu$ M; neoSTX, 1.5 nM; STX, 100 nM; TTX, 300 nM. Final liver concentration was 0.2 mg/mL.

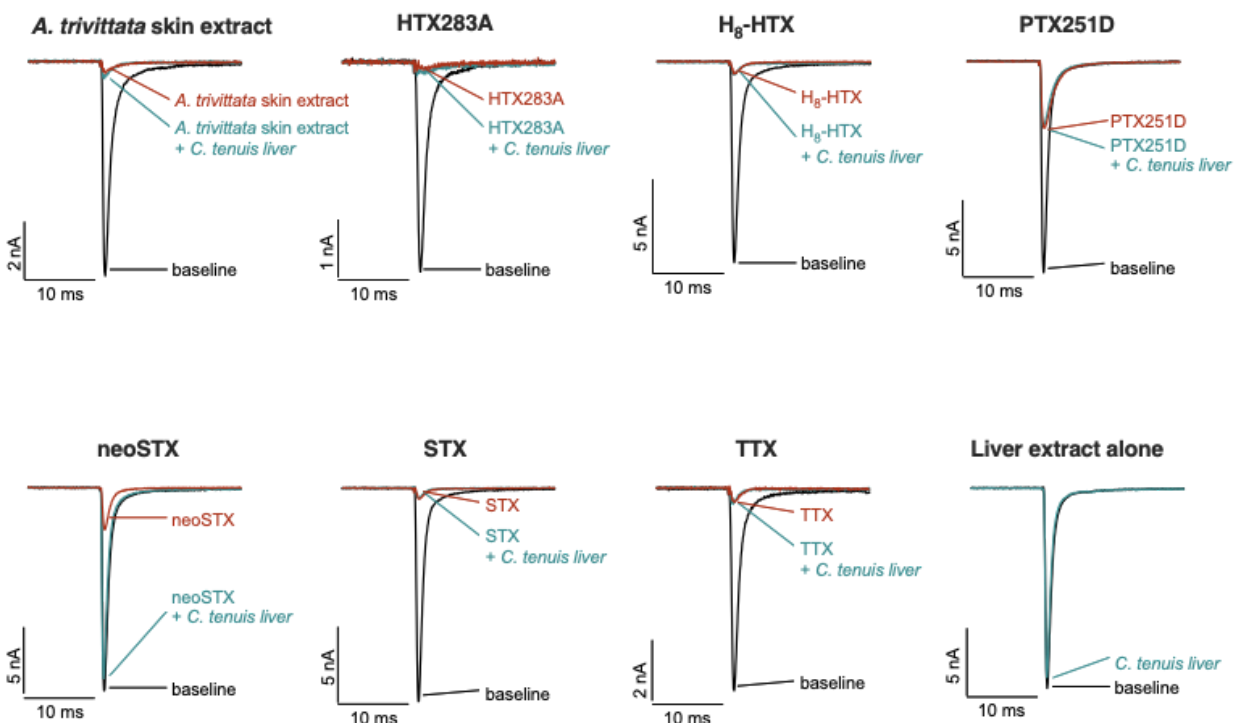


**Fig. S5. *C. tenuis* liver extract ameliorates neoSTX block of  $HsNa_v1.4$ , but does not affect STX, TTX or dendrobatid toxin block.** Exemplar whole-cell patch-clamp recordings of  $HsNa_v1.4$  expressed in CHO cells in the absence of toxin (baseline, black), presence of toxin alone (maroon), and toxin mixed with *C. tenuis* liver extract (teal). Toxin concentrations used: *A. trivittata* skin extract diluted 1:200; HTX283A, 500  $\mu$ M; H<sub>8</sub>-HTX, 250  $\mu$ M; PTX251D, 500  $\mu$ M; neoSTX, 1.5 nM; STX, 100 nM; TTX, 300 nM. Final liver concentration was 0.2 mg/mL.





**Fig. S6. Transcriptomic responses of *E. reginae* after consumption of *A. trivittata*, *S. ruber*, or under fasting conditions.** (A) Principal Component Analysis (PCA) of variance-stabilized transformed (VST) transcriptomic data from the DESeq2 package (90) across four tissues (tongue, liver, stomach, and intestine) under three dietary conditions: consumption of *A. trivittata*, *S. ruber*, or fasting. The sample Er113\_Li\_S9 correspond to the snake that died after *A. trivittata* ingestion (see Table S2). (B) Volcano plots showing differentially expressed genes across all tissues and in liver tissue for two pairwise comparisons: fasting vs. *A. trivittata* and *S. ruber* vs. *A. trivittata*. Gene families previously associated with toxin resistance were highlighted, including solute carriers (SLC), phospholipases (PLA2), cytochrome P450s (CYP), serpins (SERPIN), ATP-binding cassette transporters (ABC), heat shock proteins (HSP), Rab GTPases (RAB), cholinesterase-like genes, transferrin-related genes, lactotransferases and other *E. reginae* genes annotated in NCBI as transporters. (C) Circular plot showing liver-specific Gene Ontology (GO) enrichment analysis for upregulated genes under the cellular component category, using topGO (91). Each segment represents a GO term, with segment width corresponding to the number of upregulated genes annotated with that term (“Significant” value).



**Figure S7. *E. reginae* Na<sub>v</sub>1.4 resistant variant is sensitive to other toxins found in dendrobatid frogs (B, E, H, K, N).** Exemplar current recordings for Human Na<sub>v</sub>1.4 (*Hs*Na<sub>v</sub>1.4 in blue), and *E. reginae* Na<sub>v</sub>1.4 resistant variant (*Er*Na<sub>v</sub>1.4-R in orange) expressed in oocytes cells and exposed to (+)-pumiliotoxin 251D (PTX251D), histrionicotoxin 283A (HTX283A), (+/-)-H8-histrionicotoxin (H8-HTX), decahydroquinoline 167 (DHQ167), and decahydroquinoline 195A (DHQ195A). Comparison of sodium current reduction in the presence or absence of 500 μM PTX251D (C), 500 μM HTX283A (F), 500 μM H8-HTX (I), 1000 μM DHQ167 (L), and 1000 μM DHQ195A (O). Statistical significance was assessed using a Kruskal-Wallis test, with p-values provided for the corresponding comparisons. P-values are shown in the graph as (ns) P > 0.05; (\*) P ≤ 0.05; (\*\*) P ≤ 0.01; (\*\*\*) P ≤ 0.001.

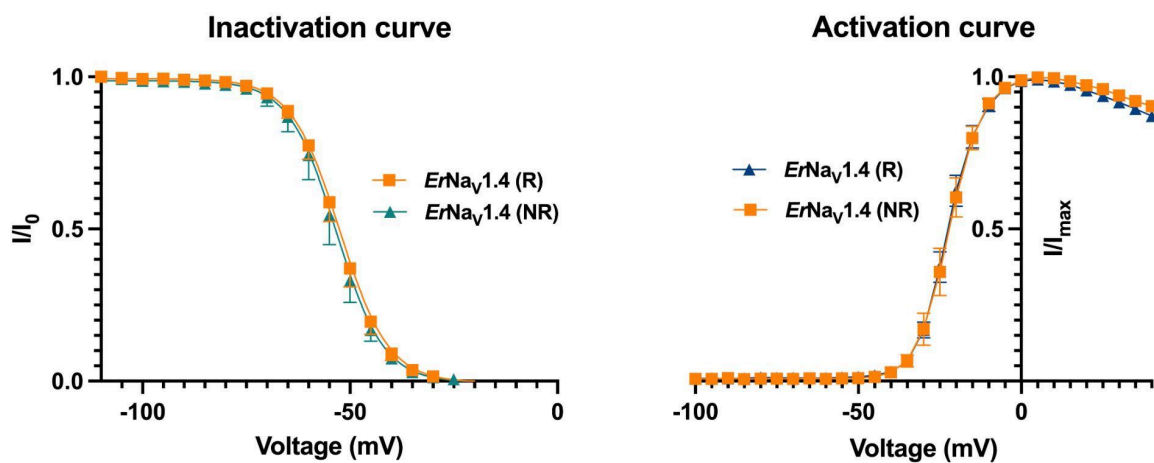


**Figure S8.** Inactivation and activation curve for the *E. reginae*  $Na_V1.4$  “resistant” (R) and “non-resistant” (NR).

Toxin	Molecular weight	Weight (mg)	Diluted in
DHQ <b>195A</b> - PTX-C	231.80524	3.8	ddH2O
DHQ <b>167</b> (PTX-CIV, HCL salt)	203.75208	3.8	ddH2O
(+)-PTX <b>251D</b> (HCL salt)	287.8685	1.8	ddH2O
(+/-)-H8-HTX (HCL salt)	327.93236	2	ddH2O
Histrionicotoxin HTX <b>283A</b>	283.4079	2	ddH2O + 5%DMSO

**Table S1.** Stock and dilution details for toxins PTX **251D**, HTX **283A**, H8-HTX, DHQ **167**, and DHQ **195A**.

<b>Toxin</b>	<b><i>HsNa<sub>v</sub>1.4</i></b>	<b><i>ErNa<sub>v</sub>1.4-NR</i></b>	<b><i>ErNa<sub>v</sub>1.4-R</i></b>
<b>TTX-TEVC</b>			
IC <sub>50</sub> (nM)	103.6 ± 28.32	18.09 ± 2.02	>>3000 nM
n	5	6	6
<b>STX-TEVC</b>			
IC <sub>50</sub> (nM)	15.56 ± 4.217	6.565 ± 1.013	>>3000 nM
n	6	4	6
<b>NeoSTX-TEVC</b>			
IC <sub>50</sub> (nM)	2.355 ± 1.170	0.4048 ± 0.235	>> 333 nM
n	6	6	6

**Table S2.** IC<sub>50</sub> values for TTX, STX, and neoSTX for *ErNa<sub>v</sub>1.4-R* “resistant” and *ErNa<sub>v</sub>1.4-NR* “non-resistant” variants, and human *Na<sub>v</sub>1.4*.

Essay	<i>ErNa<sub>v</sub>1.4 (NR)</i>	<i>ErNa<sub>v</sub>1.4 (R)</i>
<b>Inactivation</b>		
V <sub>50</sub> (mV)	-53.32 ± 3.229	-52.47 ± 2.929
K (slope)	-5.712	-5.887
K (95% CI)	-6.116 to -5.326	-6.190 to -5.592
n	12	16
<b>Activation</b>		
V <sub>50</sub> (mV)	-22.98 ± 3.382	-23.52 ± 3.554
K (slope)	4.21	3.939
K (95% CI)	3.647 to 4.810	3.508 to 4.392
n	6	14

**Table S3.** Inactivation and activation V<sub>50</sub> and slope (K) values for *E. reginae* Na<sub>v</sub>1.4-R “resistant” and *E. reginae* Na<sub>v</sub>1.4-NR “non-resistant” variants, and human Na<sub>v</sub>1.4.

## References

7. V. Ramírez-Castañeda, R. Tarvin, R. Marquez, Snakes (*Erythrolamprus* spp.) with a complex toxic diet show convergent yet highly heterogeneous voltage-gated sodium channel evolution. [Preprint] (2024). <https://doi.org/10.32942/X2MS6D>. [EcoEvoRxiv]
15. L. E. Llewellyn, P. M. Bell, E. G. Moczydlowski, Phylogenetic survey of soluble saxitoxin-binding activity in pursuit of the function and molecular evolution of saxiphilin, a relative of transferrin. *Proceedings of the Royal Society B: Biological Sciences* **264**, 891–902 (1997).
83. E. D. Brodie, M. S. Tumbarello, The Antipredator Functions of *Dendrobates auratus* (Amphibia, Anura, Dendrobatidae) Skin Secretion in Regard to a Snake Predator (*Thamnophis*). *Journal of Herpetology* **12**, 264 (1978).
84. B. L. Williams, C. T. Hanifin, E. D. Brodie, E. D. B. III, Tetrodotoxin affects survival probability of rough-skinned newts (*Taricha granulosa*) faced with TTX-resistant garter snake predators (*Thamnophis sirtalis*). *Chemoecology* **20**, 285–290 (2010).
85. S. Chen, Y. Zhou, Y. Chen, J. Gu, fastp: an ultra-fast all-in-one FASTQ preprocessor. *Bioinformatics* **34**, i884–i890 (2018).
86. S. Chen, Ultrafast one-pass FASTQ data preprocessing, quality control, and deduplication using fastp. *iMeta* **2**, e107 (2023).
87. D. Kim, B. Langmead, S. L. Salzberg, HISAT: a fast spliced aligner with low memory requirements. *Nat Methods* **12**, 357–360 (2015).
88. G. Pertea, M. Pertea, GFF Utilities: GffRead and GffCompare. *F1000Research* 9:304 [Preprint] (2020). <https://doi.org/10.12688/f1000research.23297.1>.
89. G. H. Putri, S. Anders, P. T. Pyl, J. E. Pimanda, F. Zanini, Analysing high-throughput sequencing data in Python with HTSeq 2.0. *Bioinformatics* **38**, 2943–2945 (2022).
90. M. I. Love, W. Huber, S. Anders, Moderated estimation of fold change and dispersion for RNA-seq data with DESeq2. *Genome Biology* **15**, 550 (2014).
91. A. Alexa, J. Rahnenfuhrer, *topGO: Enrichment Analysis for Gene Ontology* (2022).
92. L. E. Overman, P. J. Jessup, Synthetic applications of N-acylamino-1,3-dienes. An efficient stereospecific total synthesis of dl-pumiliotoxin C, and a general entry to cis-decahydroquinoline alkaloids. *Journal of the American Chemical Society* **100**, 5179–5185 (1978).
93. J. W. Daly, H. M. Garraffo, T. F. Spande, V. C. Clark, J. Ma, H. Ziffer, J. F. Cover, Evidence for an enantioselective pumiliotoxin 7-hydroxylase in dendrobatid poison frogs of the genus *Dendrobates*. *Proceedings of the National Academy of Sciences* **100**, 11092–11097 (2003).
94. T. Fukuyama, L. V. Dunkerton, M. Aratani, Y. Kishi, Synthetic studies on histrionicotoxins. II. Practical synthetic route to (+)-perhydro- and (+)-octahydrohistrionicotoxin. *Journal of Organic Chemistry* **40**, 2011–2012 (1975).
95. J. W. Daly, I. Karle, C. W. Myers, T. Tokuyama, J. A. Waters, B. Witkop, Histrionicotoxins: Roentgen-Ray Analysis of the Novel Allenic and Acetylenic Spiroalkaloids Isolated from a Colombian Frog, *Dendrobates histrionicus*. *Proceedings of the National Academy of Sciences* **68**, 1870–1875 (1971).



96. L. E. Llewellyn, J. Doyle, A. P. Negri, A high-throughput, microtiter plate assay for paralytic shellfish poisons using the saxitoxin-specific receptor, saxiphilin. *Analytical Biochemistry* **261**, 51–56 (1998).
97. S. F. Altschul, W. Gish, W. Miller, E. W. Myers, D. J. Lipman, Basic local alignment search tool. *Journal of Molecular Biology* **215**, 403–410 (1990).
98. OpenAI, ChatGPT (version GPT-5) (2025). <https://chat.openai.com>.

**Movie S1.** Recording of *E. reginae* feeding on *S. ruber*. Field sample number VRC19.

**Movie S2.** Recording extract of dragging behavior of *E. reginae* feeding on *A. trivittata*. Field sample number VRC101.

**Data S1. (separate file)** *E. reginae* NCBI annotation of upregulated genes across four tissues (tongue, liver, stomach, and intestine) under three dietary conditions: consumption of *A. trivittata*, *S. ruber*, or fasting. Available in dryad.

**Data S2. (separate file)** pcDNA3.1+ expression vectors containing the *E. reginae* Na<sub>v</sub>1.4 “resistant” (R) and “non-resistant” (NR), and the human Na<sub>v</sub>1.4 coding sequence. Available in dryad.

**Data S3. (separate file)** Domain IV sequences of the *E. reginae* Na<sub>v</sub>1.4 channel from field samples VRC10 and VRC09, used in the liver extract screening assay for functional toxin neutralization. Available in dryad.

**Data S4. (separate file)** Available predation experiments raw recordings. Available in dryad.

**Data S5. (separate file)** Complete manuscript in Spanish. The Spanish translation was produced using ChatGPT and edited by VRC (98) (to be uploaded after revision). Available in dryad.

**Data S6 (separate file).** General information and descriptions of the samples used in experimental assays, including museum specimen accession numbers and collection data. Available in dryad.

**Data S7 (separate file).** Samples used for transcriptome analysis, including RIN values, SRA accession numbers, experimental condition, and tissue type. Available in dryad.

**Data S8 (separate file).** List of genes annotated as transporters in the *E. reginae* NCBI genome annotation. Available in dryad.